CHAPTER 3

LATERAL SHOWER AGE PARAMETER

3.1 INTRODUCTION

The primary CR energy spectrum is known to exhibit a power law behaviour with three breaks, a '*knee*' around 3 PeV where the spectral index changes abruptly from -2.7 to about -3, an '*ankle*' at few EeV beyond which the spectrum flattens again to its original slope and a Greisen-Zatsepin-Kuzmin (GZK) suppression around 10^{20} eV (Amsler et al. 2008). Among these interesting spectral features only the *knee* is believed to be associated with solely galactic CRs. Hence measurements of the characteristics of primary CRs including its chemical composition around the *knee* are very important for proper understanding of the origin of this spectral feature as well as to get the idea about the mechanism that pushes CRs to very high energies in the galaxy. However, because of very low and steeply falling (with energy) flux, direct measurements of primary CRs on board satellites or balloons are still limited in the energy region to below a few hundred TeV. Currently the only feasible way to get information about such energetic particles on statistical basis is through the study of CR EASs, which are essentially cascades of secondary particles produced by interactions of CR particles with atmospheric nuclei.

The EAS experiments chiefly measure densities and arrival times of EAS particles in a particle detector array, mostly electrons (positrons and negatrons) and photons, at different lateral distances from which (electron) shower size and the arrival direction of EAS events are obtained. Besides, some of the other EAS components such as muons, hadrons and air shower associated Cherenkov photons are measured in conjunction with electrons. The measurements are usually interpreted in terms of shower initiating particles using detailed MC simulations, which consider interaction mechanisms of energetic particles as input. But due to the limited knowledge of particle interactions at high energies and the large fluctuations, which are intrinsic to any EAS, the conclusions on primary CRs deduced from EAS measurements remain somewhat uncertain; sometimes even there are divergences of conclusions from experiment to experiment. Recent strategies include consideration of several EAS observables simultaneously in

extracting information on primary CRs from EAS observations with lesser uncertainties.

The main parameters associated with the EAS electron component at the given observation level are the shower/electron size (N_e) which is the total number of electrons in an EAS and the lateral (or transverse) shower age ($s_\perp$) which describes the slope of the radial distribution of electrons in EAS. While shower size is often related with the energy of the EAS initiating particle but the lateral shower age has not received sufficient importance so far in deducing information on primaries from EAS observations. In the framework of the cascade theory the parameter is supposed to relate with the stage of development of EAS in the atmosphere (Kamata & Nishimura 1958).

A number of recent studies indicate that the average shape of several distributions of electrons in very high energy EAS, such as the energy distribution or angular distribution, primarily exhibits the so called *universality* (Giller et al. 2005, Nerling et al. 2006, Lipari 2009, Lafebre et al. 2009, Schmidt et al. 2008 & Gora et al. 2006): it depends only on the stage of the longitudinal shower development in the atmosphere or equivalently on the longitudinal shower age parameter ($s_\parallel$ or s_L) that represents the variation of the total number of EAS electrons with the atmospheric depth and hence describes the longitudinal shower development irrespective of the nature of the primary particle and energy. Such a feature was first divulged from the early work by Kamata and Nishimura (Kamata & Nishimura 1958) in the context of the development of CR cascades in the atmosphere and was also described in (Hayakawa 1969). The experimental data also appear to substantiate this *universality* behaviour on an average basis (Yushkov et al. 2008). The universality property is quite advantageous for the analysis of high energy CR data as it helps to parameterize the electron-positron distributions, it seems useful for an accurate estimation of the muon and electromagnetic contents in an EAS (Apel et al. 2008) and also it assists to infer the primary mass composition and the nature of the first few interactions from the observed EAS data (Yushkov et al. 2008).

The observed lateral density distribution (LDD) of EAS electrons is, however, usually described in terms of the lateral shower age ($s_\perp$), which essentially describes its slope or more precisely it gives the slope of the energy spectrum of the electron and photon populations in an EAS. Theoretically, the

relation $s_{\parallel} = s_{\perp}$ holds for both electromagnetic showers and hadron initiated EAS (Lipari 2009 & Hayakawa 1969). In most experiments, however, the estimated $s_{\perp}$ differs from $s_{\parallel}$ for an EAS with hadrons as primary. Here note that $s_{\parallel}$ can be estimated observationally only if the EAS experiment is equipped with Cherenkov or fluorescence detectors, whereas $s_{\perp}$follows immediately from the lateral distributions of electrons, which is a basic measurement of any conventional EAS array consisting of particle detectors. Hence it is imperative to explore the universality of LDD of EAS electrons in terms of the lateral shower age. In KASCADE experiments, the reconstruction procedure to lateral electron density distribution has been employed to obtain the final value of the shape parameter in place of the lateral shower age (Apel et al. 2006).

A major challenge, however, is the reliable and unambiguous estimation of $s_{\perp}$ from experimentally measured electron densities. Usually the LDD of electrons in an EAS is approximated by the well known Nishimura-Kamata-Greisen (NKG) structure function (Greisen 1956, Greisen 1960 & Snyder 1989) and the shower parameters, namely the shower size (N_e) (the total number of electrons in an EAS at an observational level) and $s_{\perp}$ are evaluated by fitting the measured densities with the NKG function. However, experimentally it is observed that the NKG function with a single $s_{\perp}$ is insufficient to describe the LDD of EAS electrons properly at all distances, which implies that the lateral age changes with the radial distance. Subsequently some modifications of the NKG structure function (Lagutin et al. 1979 & Uchaikin 1979) were proposed but the radial dependency on the shower age could not be removed totally. Under the circumstances, the notion of *local shower age parameters* (LAP) was introduced (Capdevielle & Gawin 1982, Bourdeau et al. 1980 & Capdevielle et al. 1990) which is in *essence* the lateral age at a point. Presently, different EAS groups use different structure functions and as a result, in most of the studies lateral shower age parameter is just treated as a mere parameter without assigning any physical meaning to it.

The present research work basically aims to explore for a reliable estimate of shower age parameters (lateral shower age and local age i.e. LAP) and to investigate their important characteristics and correlations with other EAS observables from a detailed MC simulation study and thereby the possible role that the parameters may play in a multi-parameter approach to studying EAS, in order to understand the nature of shower initiating particles. From this study, we have found that the shape of the radial variation of the LAP (and hence the LDD of the

electrons in an EAS) exhibits some sort of *scaling* (energy, mass and altitude independent) behaviour. It is noticed here that the shape of the radial variation of the LAP is, however, found to depend on the choice of the effective Moliére radius in the NKG function. Such a *scaling* feature provides a better description of the radial electron distributions in EAS and should help to estimate the electron content in an EAS accurately.

3.2 SHOWER AGE PARAMETERS

The most simple and earliest description of the electromagnetic cascade was starting with the longitudinal development. The average longitudinal profile of an electromagnetic cascade, which is developed in a medium through a multiplicative process involving the interactions of electrons and photons when passing through it, was provided by Greisen (Greisen 1956, Greisen 1960 & Snyder 1989) on the basis of the calculations of Snyder carried in the so called *Approximation B* (taking into account only three processes of pair-production by the photons, bremsstrahlung by the electrons and the ionization loss suffered by the electrons while neglecting the Compton scattering)

$$N_e = \frac{0.31}{\sqrt{ln(\frac{E_0}{\epsilon_0})}} exp[t(1 - 1.5ln(s_{||})]. \qquad (3.1)$$

Here E_0 is the energy of the primary photon generating the cascade, ϵ_0 is the critical energy (below which ionization losses predominate over that due to pair production) with a value of ~82 MeV. Note that t is expressed here in cascade units (the atmospheric depth has been divided by the electron radiation length in air, taken as 37.1 gm-cm^{-2}). In this useful synthesis a very simple parameterisation of the longitudinal age $s_{||}$ is defined by the relation

$$s_{||} = \frac{3t}{t + 2ln(\frac{E_0}{\epsilon_0})} . \qquad (3.2)$$

As mentioned already the development stage of a pure electromagnetic cascade is characterized by the single age parameter $s_{||}$, known as longitudinal shower age. Mathematically, it was determined earlier as the saddle point in the inverse Mellin transformation of cascade transport equation as indicated by the

previous works in the more simple *Approximation A* (taking into account only the radiation process and the pair creation in their asymptotic forms at high energy). The lateral development was described by Nishimura and Kamata solving by the three dimensional diffusion equations (see *Appendix A*) after the preliminary work of Moliére and Bethe focused on the lateral electron distribution near the cascade maximum. Fitting their numerical results on the electron densities at a distance r from the shower axis, Nishimura and Kamata were able to propose a first semi-analytic lateral distribution in a shower age $s_{\|}$. Under *Approximation B* and taking into account the hegemony of the multiple Coulomb scattering for the lateral deflections electrons, an expression of radial distance dependence of $s_{\|}$ was inferred in the simple form (Kamata & Nishimura 1958),

$$s_{\|}(r) = \frac{3t}{t + 2ln\left(\frac{E_0}{\epsilon_0}\right) + 2ln\left(\frac{r}{r_m}\right)} \qquad (3.3)$$

where r is the radial distance from the shower core and r_m is the Moliére radius (near 80 m at sea level) which is a characteristic constant of a medium defined as the radius of a cylinder containing on average 90% of the electromagnetic showers energy deposition (it is the natural lateral displacement unit in air corresponding to a thickness of 9.4 $gm\text{-}cm^{-2}$: the last value comes from the calculation of the mean scattering angle in the case of multiple Coulomb scattering with a scattering energy $E_S = 21\ MeV$). With the identification $s_{\|} = s(r)$ when $r = r_m$, $s_{\|} = 0$ at the origin of the cascade and $s_{\|} \sim 1$ at the shower maximum.

In the same theoretical context the lateral density distribution of cascade particles given by Nishimura and Kamata can be approximated by the well known *Nishimura-Kamata-Greisen* (NKG) structure function proposed by Greisen (Greisen 1956 & Greisen 1960), given by

$$f(r, s_{\perp}) = C(s_{\perp})(\frac{r}{r_m})^{s_{\perp}-2}(1 + \frac{r}{r_m})^{s_{\perp}-4.5}, \qquad (3.4)$$

where the normalization factor $C(s_{\perp})$ is given by

$$C(s_{\perp}) = \frac{\Gamma(4.5 - s_{\perp})}{2\pi r_m^2 \Gamma(s_{\perp})\Gamma(4.5 - 2s_{\perp})}. \qquad (3.5)$$

The NKG formula has the advantage of normalization as it is integrable in Euler Beta function provided $s_{\perp}$ is independent of r. The normalisation of $f(r)$

implies that $\rho(r) = N_e f(r)$, $\rho(r)$ being the electron density at r (thanks to the properties of the Eulerian function as shown in *Appendix A*).

The relation $s_{\parallel} = s_{\perp}$ was considered to hold for pure electromagnetic showers (Kamata & Nishimura 1958). Such equivalence implies the correlation between steeper lateral distributions ($s_{\parallel} < 1$) or flatter lateral distributions ($s_{\parallel} > 1$) in proportion to the distance to shower maximum; it suggests also the employment of the observable $s_{\perp}$ as a hint of the global shower cascading expected to depend on primary mass and interaction features (cross-section, multiplicity and inelasticity). Hence, the equations (**3.1**), (**3.2**) and (**3.4**) together provide an attractive and a complete procedure of calculating the $3D$ development of the electromagnetic cascade (as first pointed out by Cocconi (Cocconi 1961)).

The superposition of many such pure electromagnetic cascades build the electron component of a hadron initiated EAS. It was also suggested (Kamata & Nishimura 1958, Lipari 2009) that for hadron initiated EAS, both the longitudinal structure and lateral structure of soft components can be described by that of a resulting single cascade, assigning a suitable value to the age parameter. Recent MC simulation studies (Giller et al. 2005, Nerling et al. 2006 & Lafebre et al. 2009) exhibited a possible universality for large EAS with primaries in the EeV energy range in terms of longitudinal age defined through the relation (**3.2**).

However Nishimura, Kamata and Greisen noted some difficulties when comparing the prediction of the cascade theory with the measured lateral electron distributions in EAS and we have listed hereunder some limitation on the validity of the analytical expressions caused by the various approximations in obtaining the solutions as well as due to over-simplification of the adopted $3D$ transport equations. The conditions of validity of relation (**3.4**) are

- $E_0/\epsilon_0 \gg 1$ due to the asymptotic value of the cross-sections.
- $t > 1$ (more than one radiation unit is necessary to consider the continuity in the cascade).
- $|\log(E_0/\epsilon_0)| \gg |\log(r/r_m)|$.

The last condition may be not fulfilled near the shower axis as underlined by Nishimura considering not appropriate to use the data near the shower core.

Nishimura and Kamata have also ascertained that corrections where necessary to their calculations performed for the homogeneous medium. In consequence, taking into account the variation of the air density, they have inferred that in order to compare the theoretical curves with the experimental data, the distribution obtained at about 2 radiation length (in the case of *Approximation B*) above the measurement area has to be employed.

Furthermore, Nishimura ascertained again that near the shower axis the densities were quite lower with NKG than with the original NK formula (Nishimura 1967) for $s \geq 1.2$. Greisen also noticed larger densities in experimental measurements than that given by NKG far from the axis (Greisen 1956, Greisen 1960 & Snyder 1989) which was inferred as a possible contribution of the muon decay. A shorter value of the second momentum of the distribution than in the NKG was observed by Allan for the lateral structure (Allan et al. 1975) and a couple of years later a steeper profile was exhibited by Hillas and Lapikens from MC calculation near 100 GeV (Hillas & Lapikens 1977).

Simultaneously, the $3D$ diffusion equations were solved using adjoint equations, the Bessel Fourier transformation being applied to r and the numerical integration on t and on the energy E being performed by partial polynomial functions (Lagutin et al. 1979 & Uchaikin 1979). This method, which involves several approximate steps and numerical inverse transformations, leads to a limiting (as $E_0 \rightarrow \infty$) radial distribution. An improvement of the NKG function was proposed by adopting a modulated, longitudinal age parameter $s_{\parallel}$ dependent effective Moliére radius so that

$$\rho_{el} = (mr_m)^{-2}\rho_{NKG}(r/m) \qquad (3.6)$$

where $m = 0.78 - 0.21s_{\parallel}$.

We underline here that it is ρ_{el} and not only ρ_{NKG} which has been implemented in the so called subroutine NKG of CORSIKA. The procedure of calculation is the following: N_e is calculated together with $s_{\parallel}$ (via Greisen formula) for each sub-cascade generated by one photon after one pair creation by one secondary of one hadron interaction in the EAS. The electron component is subsequently obtained from the sum of the densities at one given distance of the individual axis of each sub cascade (Capdevielle & Gawin 1982, Bourdeau et al.

1980 & Capdevielle et al. 1990). Of course the procedure doesn't distinguish e^+ and e^- and the annihilation of the positron is not considered.

On the other hand, observing that the experimental LDD of electrons in EAS was steeper than that given by the ρ_{NKG} and was in better agreement with the MC calculations of Hillas (Hillas & Lapikens 1977) at lower energies. Capdevielle *et al* (Capdevielle & Gawin 1982, Bourdeau et al. 1980 & Capdevielle et al. 1990) introduced the notion of *local age*. After testifying the behaviour of the LAP on experimental lateral distributions and reaffirming it with the Akeno observations (Nagano et al. 1984[b]), this approach was validated by the *rapporteurs* of the *International Cosmic Ray Conferences* during the period 1981 to 1985 (Tonwar 1981, Rao 1983 & Clay 1985). The whole procedure was also employed in the calculation of the radio effects of EAS (Suprun et al. 2003).

From two neighbouring points, i and j, we can give the (*local*) *lateral age* parameter (s_{ij}^{local}) for any NKG like distribution $f(x)$ (where $x = r/r_m$) which characterises the best possible description for the electron LDD in $\{x_i, x_j\}$:

$$s_{ij}^{local} = \frac{\ln (F_{ij} X_{ij}^2 Y_{ij}^{4.5})}{\ln (X_{ij} Y_{ij})} \qquad (3.7)$$

where $F_{ij} = f(r_i)/f(r_j)$, $X_{ij} = r_i/r_j$ and $Y_{ij} = (x_i + 1)/(x_j + 1)$. More generally, $r_i \to r_j$, this suggests the definition of the LAP $s_{\perp}^{local}(x)$ at each point:

$$s_{\perp}^{local}(x) = \frac{1}{2x+1}\left((x+1)\frac{\partial lnf}{\partial lnx} + (2+\beta_0)x + 2\right) \qquad (3.8)$$

If $\beta_0 = 4.5$, $f_{NKG}(r)$ with $s_{\perp} \equiv s_{\perp}^{local}(r)$ can be used to fit f in the neighbourhood of r.

Typical behaviour was predicted with a characterized minimum value of $s_{\perp}^{local}(r)$ near about 50 m from the axis, followed by a general increase at a large distance (Capdevielle & Gawin 1982, Bourdeau et al. 1980 & Capdevielle et al. 1990). The relation $s_{\perp}^{local}(r) \equiv s_{ij}^{local}$ for $r = (r_i + r_j)/2$ was found to be valid for the experimental distributions (taking $F_{ij} = \rho(r_i)/\rho(r_j)$ as far as they were approximated by monotonic decreasing functions versus distance).

Such a prediction was substantiated by Akeno (Nagano et al. 1984[b]), North Bengal University (NBU) EAS experiments (Sanyal et al. 1993) and other

experiments (Capdevielle & Gawin 1982, Bourdeau et al. 1980 & Capdevielle et al. 1990). The LAP depends mainly on the logarithmic derivative of the density versus the distance as it appears in the relation (**3.8**); however, this pure mathematical approach may not be attained in practice at any radial distance, due to the experimental uncertainties arising mainly from the use of a finite number of detectors for the density measurements, triggering conditions and errors in the determination of the shower core position. Therefore, $s_{\perp}^{local}(r)$ is estimated via the relation (**3.7**) using physical bands of distance $\{r_i, r_j\}$; for experiments with very dense grids of detectors, such distance bands may be reduced to 5 - 10 m, but they may have to enlarge up to about 20 m for arrays with a lower resolution, as well as in the case of individual showers with large fluctuations. For very large and giant EAS, the interval $\{r_i, r_j\}$ may be required to exceed 100 m or so. We preferred to conserve the characteristic parameters of electro-magnetic cascade in relation (**3.7**) including the value of the Moliére radius to facilitate the comparison with the experimental data, which is most frequently expressed in NKG formalism.

The dependence of $s_{\perp}^{local}(r)$ on r rules out a consistent integration via relation (**3.4**) casting some doubt on the accurate relation between density and size; it was shown that such a dependence on $s_{\perp}^{local}(r)$ on r is mainly a basic feature of pure electromagnetic cascades (Capdevielle & Gawin 1982, Bourdeau et al. 1980, Capdevielle et al. 1990 & Bhadra 1999).

Furthermore, the observed lateral density distribution of air shower electrons is usually described in terms of lateral structure function and hence in terms of lateral shower age and in most experiments the estimated transverse shower age ($s_{\perp}$) differs from the longitudinal age ($s_{\parallel}$) for EAS with hadrons as primary. It was suggested from the experimental results (Dedenko et al. 1975 & Stamenov 1987) that these two age parameters are connected through the (approximate) relation $s_{\parallel} \geq s_{\perp} + \delta$, with $\delta \approx 0.2$. Some early MC simulation results obtained a relation of the nature $s_{\parallel} \sim 1.3 s_{\perp}$ (Capdevielle & Gawin 1982, Bourdeau et al. 1980 & Capdevielle et al. 1990), $s_{\perp}$ being derived from density measurements around 50 m from axis. Here note that the longitudinal age can be estimated observationally only if EAS experiment is equipped with Cherenkov or fluorescence detectors, whereas the lateral shower age parameter follows straightway from the LDD of electrons which is the basic measurement of any conventional EAS array consisting of particle detectors.

3.3 METHOD OF SIMULATION

For generating EAS events, the air shower simulation program CORSIKA (Heck et al. 1998 & Capdevielle 1992) is exploited here. Here our discussions are mainly restricted to CRs in the knee region of the primary spectrum. In the present work, the high energy (above 80 GeV/n) hadronic interaction model QGSJET **01** version **1c** (Kalmykov et al. 1997) was used in combination with the low energy (below 80 GeV/n) hadronic interaction model GHEISHA (version **2002d**) (Fesefeldt 1985) or FLUKA (Fass`o 2001), depending on the primary energy in the framework of the CORSIKA MC program version **6.600/6.970** (Heck et al. 1998 & Capdevielle 1992) to generate EAS events. Note that the low energy interaction model GHEISHA exhibits a few shortcomings (Drescher et al. 2004, Bhadra et al. 2009, Heck 2006 & Ferrari et al. 1996) but the LDD of EAS electrons does not depend much on the low energy hadronic models, except at large distances (Drescher et al. 2004). Hence for very high energy events involving large radial distances we employed FLUKA (Fass`o 2001). A relatively smaller sample was also generated using the high-energy interaction model SIBYLL **v2.1** (Fletcher et al. 1994) to judge the influence of the hadronic interaction models on the results.

The CORSIKA program allows one to choose either of the two options, the EGS4 (electron gamma shower system version **4**) (Nelson et al. 1985) and the NKG for obtaining a lateral distribution of the charge particles. The former option facilitates a detailed MC simulation of the electro-magnetic component of a shower that incorporates all the major interactions of electrons and photons (Rossi & Greisen 1941), whereas the NKG option relies on an analytical approach rather than a full MC simulation. In the NKG option, the electron density of an electro-magnetic sub-shower is calculated straightway using the NKG function with a reduced Moliére radius (Lagutin et al 1979, Capdevielle & Gawin 1982, Bourdeau et al. 1980 & Capdevielle et al. 1990). One gets better accuracy and more detailed information about the electro-magnetic component with the EGS4 option, at the expense of long computing time. We underline here that the NKG option (subroutine NKG inside CORSIKA) is dealing mainly with the relations (**3.6**) and (**3.7**) and not directly with equation (**3.4**). Furthermore the reference (Capdevielle et al. 1977) in CORSIKA original documentation was mismatched with the appropriate references (Capdevielle & Gawin 1982, Bourdeau et al. 1980 & Capdevielle et al. 1990). It was unfortunately reproduced in the user's guide and in

several papers, for instance (Antoni et al. 2001) generating a confuse interpretation of the NKG option.

We have considered the US-standard atmospheric model (NASA report 1976) with a planar approximation. The maximum primary zenith angle was restricted to 50^0 for the present study. The EAS events were generated mainly for proton and iron nuclei as primaries. A few events were also generated for gamma-ray as primary. Irrespective of the nature of the primaries, the slope of primary power law spectra was taken as -2.7 below the knee i.e. 3×10^{15} eV and as -3.0 above. The EAS events were simulated at different geographical positions corresponding to the experimental sites of Akeno (Nagano et al. 1984[b]), KASCADE (Antoni et al. 2001) and NBU (Bhadra et al. 1998). The magnetic fields are provided accordingly. On the observation level, the kinetic energy thresholds were chosen as 3 MeV for electrons (e^+ and e^-) irrespective of the primary species and energies.

3.3.1 GENERATION OF THE EAS MONTE CARLO LIBRARY

The simulated shower library consists of more than 30 000 EAS events with the EGS4 option and more than 180 000 events with the NKG option in the primary energy interval of 10^{14} eV to 3×10^{16}eV. In order to appreciate the asymptotic tendencies at ultra high energies, our library has also been enriched by about 1000 events simulated at $E_0 = 5 \times 10^{17}$ and 10^{18} eV for proton and iron primaries: apart from the thinning factor which is taken as 10^{-6} with optimum weight limitation (Kobal 2001) (i.e., all particles are followed up to an energy E_{th}, where $E_{th}/E_0 = 10^{-6}$, after which only one of those particles is tracked giving appropriate weight to it) the simulation conditions are here identical concerning the hadronic interaction models, the zenith angle range, both the EGS4 and the NKG options. Here we would like to specify that the optimized thinning factor 10^{-6} with the optimum weight limitation for the CORSIKA version used here is considered as the best compromise between the computing time and the accuracy at high energies (Knapp et al. 2003).

In all cases involving the EGS4 option, the longitudinal development is restored numerically and that the longitudinal age parameter is computed (Capdevielle & Cohen 2006[a], 2006[b]), instead of relation (**3.2**) by

$$s_{||} = \exp\left[\frac{2}{3} \times \left\{1 + \frac{\alpha}{t} - \tau\right\}\right] \; with\, \tau = \frac{t_{max}}{t}, \alpha = ln\frac{N_{max}}{N_e} \qquad (3.9)$$

where t_{max} and N_{max} are respectively depth and size read at the cascade maximum. In relation (**3.9**), N_e represents the electron size at the atmospheric depth t which is usually expressed in cascade units.

3.3.2 THE NKG AND THE EGS4 OPTIONS

Taking the opportunity of CORSIKA to calculate the electromagnetic component of EAS via the EGS4 and the NKG procedure, we have used both the options simultaneously for about 30 000 events. In **Fig.3.1** we compare the LDD of EAS electrons obtained with the stated two options for proton, iron and gamma-ray primaries. It is clear from the figure that the NKG option gives a higher density with steeper radial distribution compared to the EGS4 option. A small density excess appears for the pure electro-magnetic cascades near the axis for the NKG options; such an excess presents also in the proton initiated air showers. However, for the proton showers, a tolerable agreement between the output of the two options was noted over a large band of densities between radial distances of $10 - 100$ m from the shower axis; it reconfirms that for proton and photon initiated showers the NKG option is quite useful to calculate a large number of cascades in a short time.

For iron primaries, both the options indicate an older density profile near the axis. The NKG option was found to give an excess density between $2 - 10$ m distances. The average energy of the positrons was quite a bit lower in the case of iron initiated showers and the cross section of positron annihilation becomes more important for the lower part of the cascade. This effect is probably enhanced by the longer path of the electrons in the geomagnetic field and the larger energy loss by ionization. The NKG option is, therefore, not so accurate for the simulation of heavy nuclei initiated showers with large zenith angles after the shower maximum. For vertical showers, the output of the NKG option is nevertheless acceptable. At larger distances a slight deficit in the densities appears with the NKG option; this probably comes from the different treatment of the multiple Coulomb scattering in the NKG option than in the EGS4. Furthermore, Bhaba and Moller scattering are treated in complement with the separated MC procedures. On the other hand, the geomagnetic field of the earth enhances the path of the muons as well. Consequently their losses by ionization and their decay give more electrons, which

were not incorporated in the NKG option. Besides, the NKG option does not accommodate photo-production inside the electro-magnetic sub cascades as the EGS4 code itself contained.

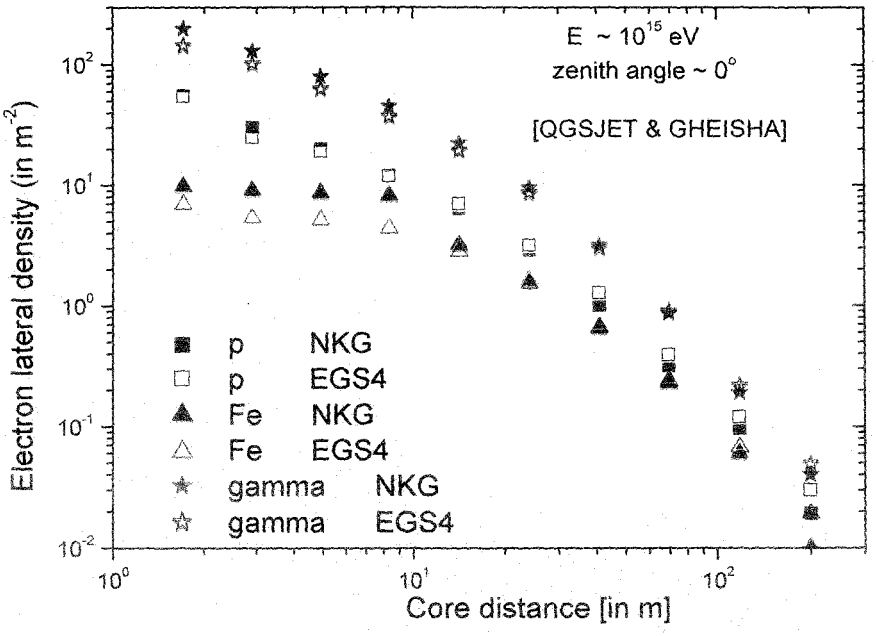

Fig.3.1: Comparison of the EGS4 and the NKG generated lateral distribution of electrons for different primary cosmic ray species. The statistical errors are within the dimensions of the symbols used.

3.4 ESTIMATION OF SHOWER AGE

The simulated data have been analyzed using the reconstruction algorithms developed to obtain shower size and shower age (called basic shower parameters). We adopt two different methods. First following the traditional approach we estimated basic shower parameters by fitting density data with the NKG structure function. Secondly, exploiting equation (**3.7**) we directly estimate local age parameter for each individual event.

3.4.1 LATERAL AGE THROUGH NKG FITTING

In this approach the simulated electron densities at radial distances have been fitted by the method of chi-square minimization through an iterative procedure based on the method of steepest decent to the NKG lateral distribution function of electrons. Here it is to be noted that majority of the EAS groups traditionally estimate basic shower parameters based on the NKG function. In

order to check the goodness of the NKG function in describing the simulated radial density distribution of electrons we first fitted the simulated density data at various radial distances with the NKG function and compare radial density distribution for simulated events with the fitted curve. In **Figs. 3.2a – 3.2c** the simulated particle densities at different radial distances are plotted along with the fitted curves obtained with the NKG function.

As mentioned already the NKG function with a single age cannot describe the EAS particle densities properly over a reasonable radial distances from the shower core. This is reflected in **Fig.3.2a** where the average electron densities over a radial distance range up to about 5800 m from the shower core obtained with the EGS4 option at primary energy 5×10^{17}eV at the geographical site of KASCADE is fitted with the NKG structure function with a single lateral age $s_{\perp}$. The limits in the employment of NKG at very high energy came from both asymptotic representations by simple power laws when $r \rightarrow 0$ and $\rightarrow \infty$. This difficulty in Akeno was reduced by introducing the sum of a pair of NKG functions and in KASCADE by an important reduction of Moliére radius as in earlier experiments at high altitude. A more general function than the Eulerian approach was also proposed in terms of Gaussian hyper-geometric function (Capdevielle & Cohen 2006[a]. 2006[b]) to describe accurately the lateral electron distribution.

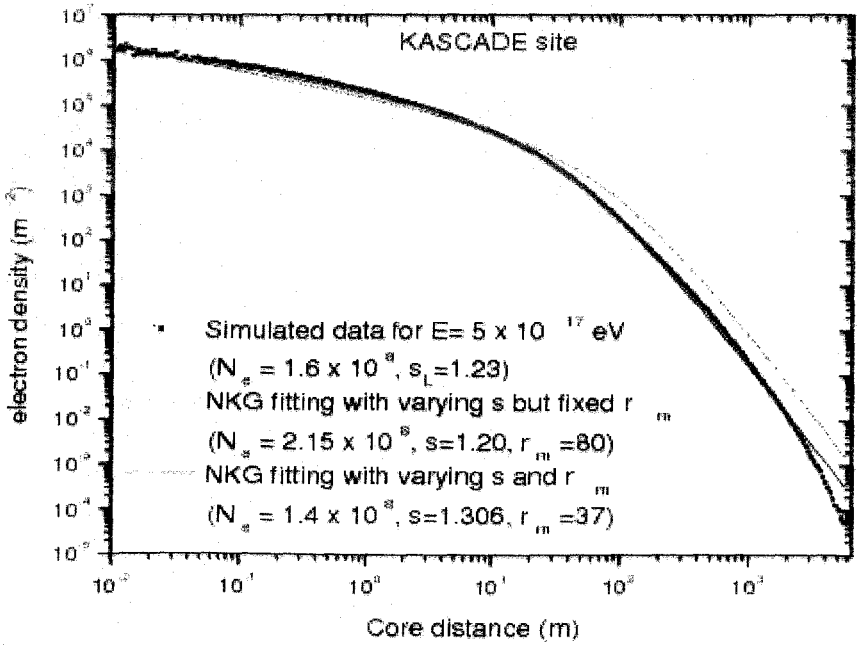

(a)

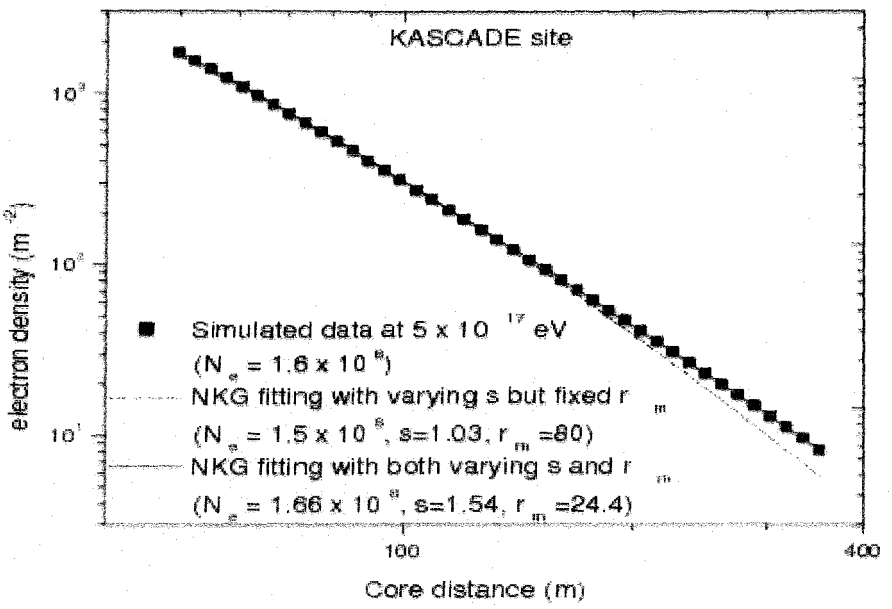

(b)

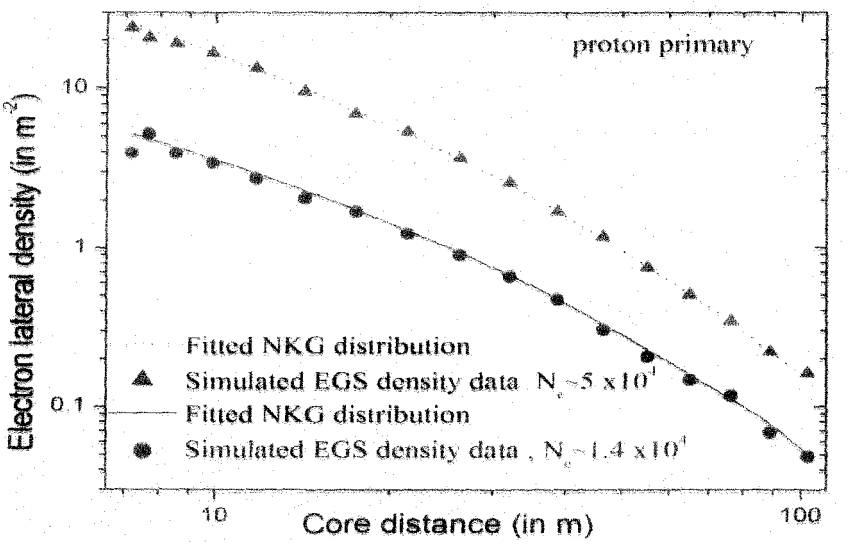

(c)

Fig.3.2: (a) NKG fitting of the EGS4 output of electron density at KASCADE site for p primary covering radial distance more than 5000 m, (b) the same as Fig.3.2a but restricting radial distance between 50 – 350 m and (c) NKG fitting with a constant single age of the EGS4 output of electron density at NBU site restricting radial distance only up to 100 m. The statistical errors are within the dimensions of the symbols used.

We also noted that the description of the data by the NKG function is improved a lot when the Moliére radius is treated as a variable rather than a fixed parameter which is also shown in the same figure. But this better description comes at the expense of very high lateral shower age value which somewhat obscures the physical meaning of the age parameter as assigned in the cascade theory.

In the **Fig.3.2b** we did the same fittings as in **Fig.3.2a** but restricting the radial distance to the range 50 to 350 m. The reason for such a restriction on the radial distance will be clear at the end of this section **3.4**. Here again it is found that the Moliére radius as a free variable improves the description of the simulated data considerably. For small EAS arrays where the radial distance is limited to about 100 m or so, the NKG structure function is found to represent the simulated data reasonably well except at very small distances as is shown in **Fig.3.2c** for two shower size ranges. At very small distances the simulated densities are found higher than those given by the NKG function. The simulated particle densities only in the radial interval 7 - 100 m are thus finally considered for parameter reconstruction and fitted showers with reduced chi square ($\chi^2_{red.}$) less than 5 are only accepted for results on characteristics of shower age parameter.

The error in estimating lateral shower age in the shower size interval 10^3 – 10^5 particles (corresponding to the primary energy range 10^{14} – 3×10^{15} eV) was found to be ±0.03 for the QGSJET model and ±0.05 for the SIBYLL. The larger error for the SIBYLL model seems solely statistical, due to the generation of a relatively fewer number of EAS events using the latter model.

3.4.2 LOCAL AGE PARAMETER

The local age for EAS charged particles was computed for each individual event straightway, applying equation (**3.7**). When estimating the LAP, the main sources of error are the fluctuations in particle density and the uncertainties in radial distance estimation. In simulated data the radial distance of each particle is known with a high accuracy. In this work the error in the LAP, due to uncertainties in radial distance estimation was kept small by taking small radial bins. For minimizing the statistical fluctuations in particle density at different radial bins, a large number of events need to be considered. In this analysis, the error of the LAP for EAS with the primary energy in the PeV range remains within 0.05 for $10\,m < r < 250\,m$, whereas for $r < 10$ m or when $r > 300$ m the error of the LAP is found to be higher, about 0.1. At higher primary energies

(5×10^{17} – 10^{18} eV) the error of the LAP is found at about 0.12 near the core, which decreases to about the 0.07 level when $20\,m < r < 300\,m$ but increases again with the radial distance and reaches to about 0.15 when r approaches $1000\,m$.

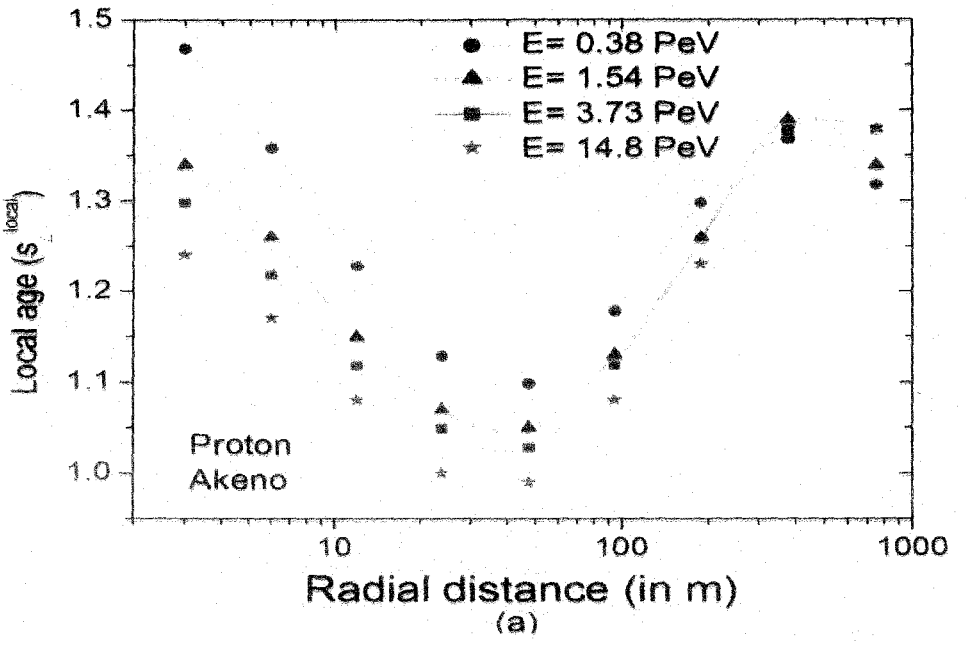

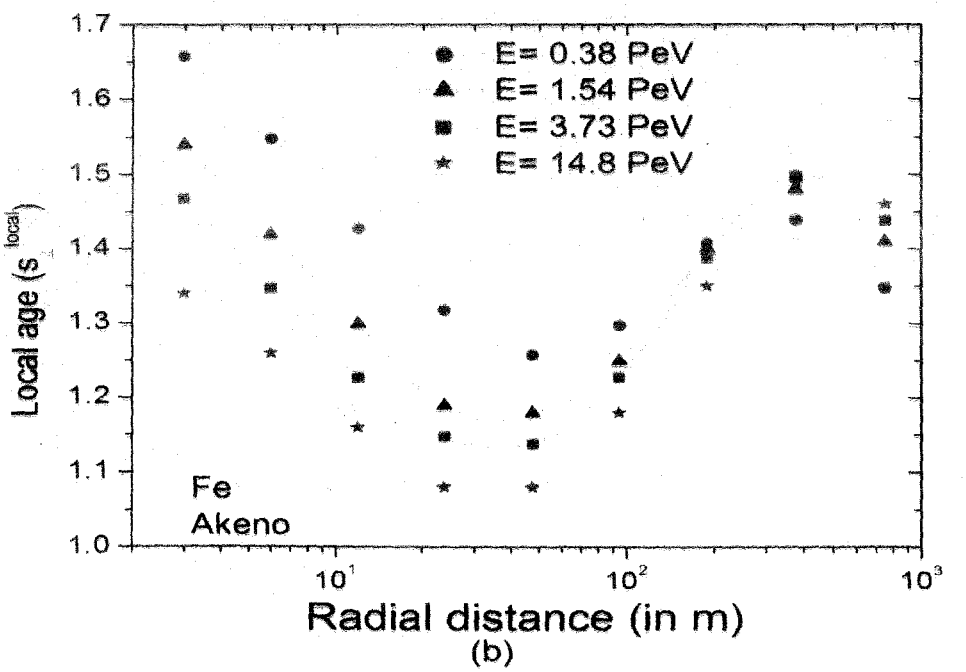

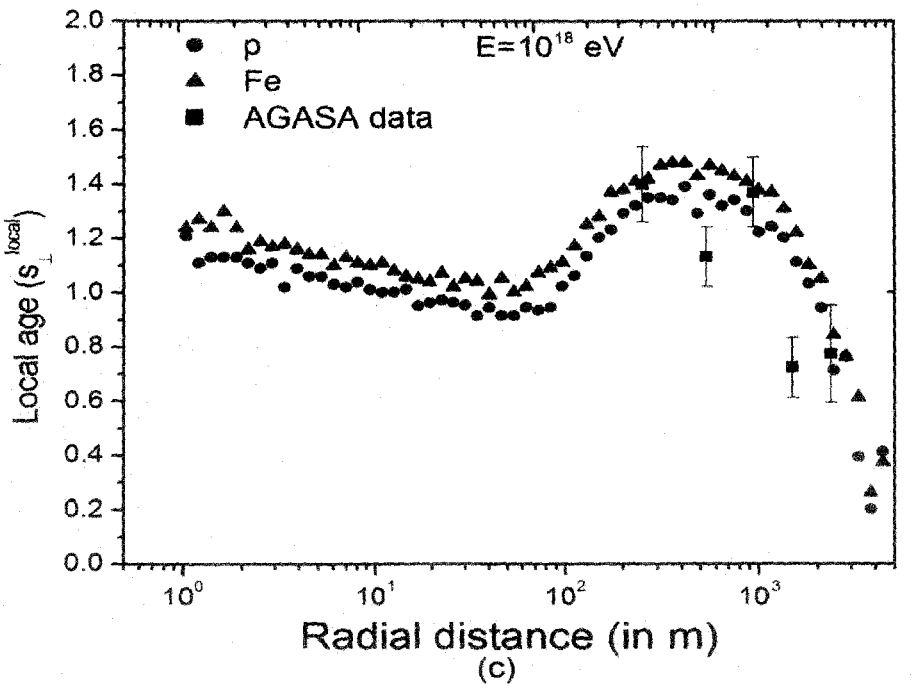
p
Fe
AGASA data
E=10^18 eV
Local age (s^local)
Radial distance (in m)

(c)

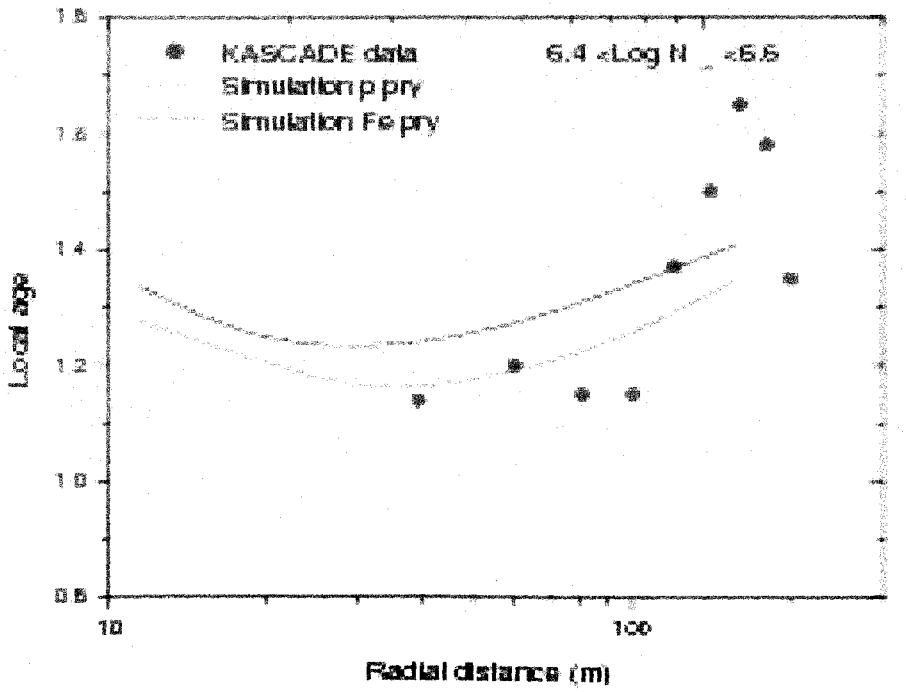
KASCADE data
Simulation p pry
Simulation Fe pry
Local age
Radial distance (m)

(d)

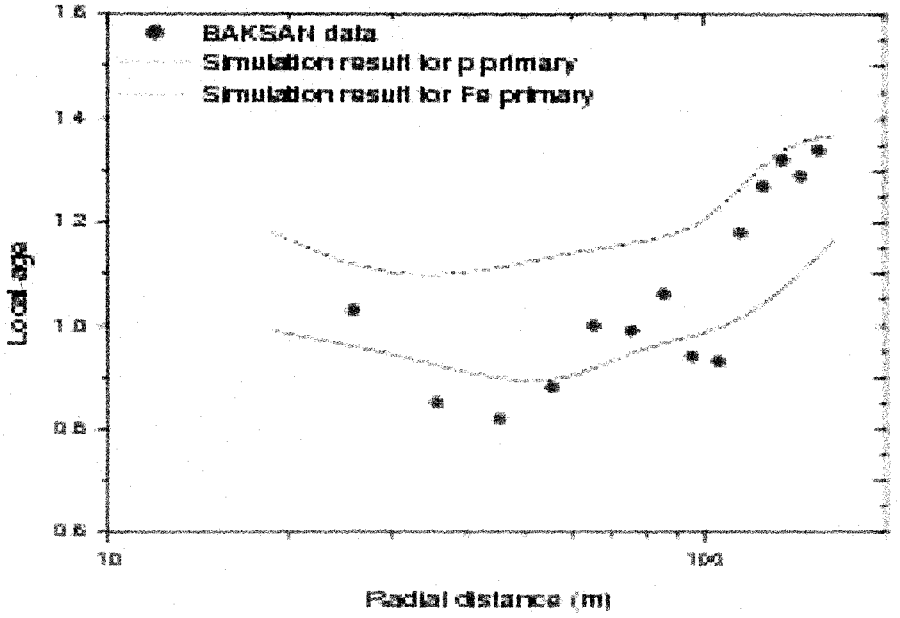

(e)

Fig.3.3: Variation of the LAP (estimated from the simulated data) with radial distance for different primary energies at Akeno site (920 gm-cm^{-2}) for (a) proton (b) iron and (c) for both p and Fe along with the local age obtained from the experimental data. The lines are only a guide for the eye. The same studies are also made for KASCADE and BAKSAN experimental data as shown in Figs. (d) and (e).

The variation of the LAP with the radial distance from the shower core is shown in **Fig.3.3**. It is known from previous studies (Capdevielle & Gawin 1982, Bourdeau et al. 1980 & Capdevielle et al. 1990) that with an increase of the radial distance, the LAP initially decreases, reaching a minimum at around 50 m and then increases, as was also noted from the experimental data (Nagano et al. 1984[b] & Sanyal et al. 1993). Here we noticed two other interesting features (**Figs.3.3a – 3.3e**): the local age again starts to decrease at around 300 – 400 m. To examine whether the experimental data also demonstrates a fall in the local age at large radial distances, we compute the local age from the LDD data of total charged particles, as measured by the AGASA experiment (Yoshida et al. 1994) for primary energy 2×10^{18} eV and compared these values with our simulation results in **Fig.3.3c** using EGS4 output. The experimental data clearly support the trend predicted by the simulation results at larger radial distances. The characteristic high-low-high kind of radial variation in the local age at relatively smaller

distances (within 300 m or so) could not be substantiated by the AGASA data, due to the large separation of the detectors of the array. Here due to limited statistics the position of the minimum of the local age could not be located with good precision but the overall nature of the radial dependence of local age is found the same to that at lower energies. It is worthwhile mentioning that there was an indication for such a decrease of $s_{\perp}^{local}(r)$ at around 300 m in the experimental results obtained by Akeno (Sanyal et al. 1993) and KASCADE-Grande (Ulrich et al. 2008 & 2009[a]). Such behaviour is also depicted in **Fig.3.4** of the KASCADE report (Antoni et al. 2001), where one may notice a maximal deficit at 50–80 m in the ratio of the measured and the fitted electron densities and an excess at larger distances when fitted with the NKG formula. Here we have compared the radial variation of LAP obtained out of the simulated data for proton and iron primaries with those obtained from the experimentally measured density data of KASCADE and BAKSAN (Voevodsky et al. 1993) in **Figs.3.3d – 3.3e** respectively.

These findings are important for an analysis of very large air showers observed/to be observed by the KASCADE-Grande, AGASA, AUGER, Yakutsk and Telescope Array involving large radial distances. The large EAS experiments often treat charged particle densities at large radial distances, such as 500, 600, 1000 m from the shower core as an estimator of the primary particle energy, though such a technique involves several uncertainties (Capdevielle et al. 2009). These findings of a rapid change in the slope of the radial distribution of electrons at large radial distances, suggest that more controls should be adopted in the estimation of the primary energy of large showers, for instance by taking particle densities at more than one radial distance.

Another important observation is that in general the nature of the variation of the local age with the radial distance appears nearly the same for all of the primary energies, *i.e.* the nature of the variation is practically independent of the energy of the shower initiating particles, which implies that the local age (or the lateral distribution of electrons in EAS) exhibits some sort of *scaling* behaviour in respect to the radial dependence from the shower core. This feature of the local age is maintained even for different primary species and observational levels.

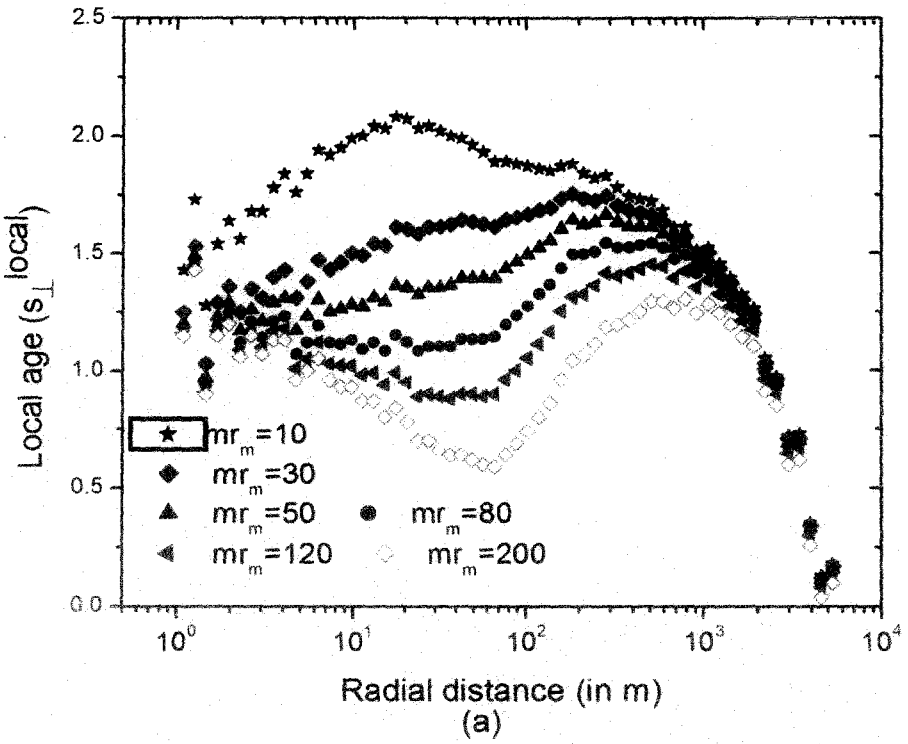
Local age ($s_\perp^{local}$)
Radial distance (in m)
mr_m=10
mr_m=30
mr_m=50
mr_m=80
mr_m=120
mr_m=200

(a)

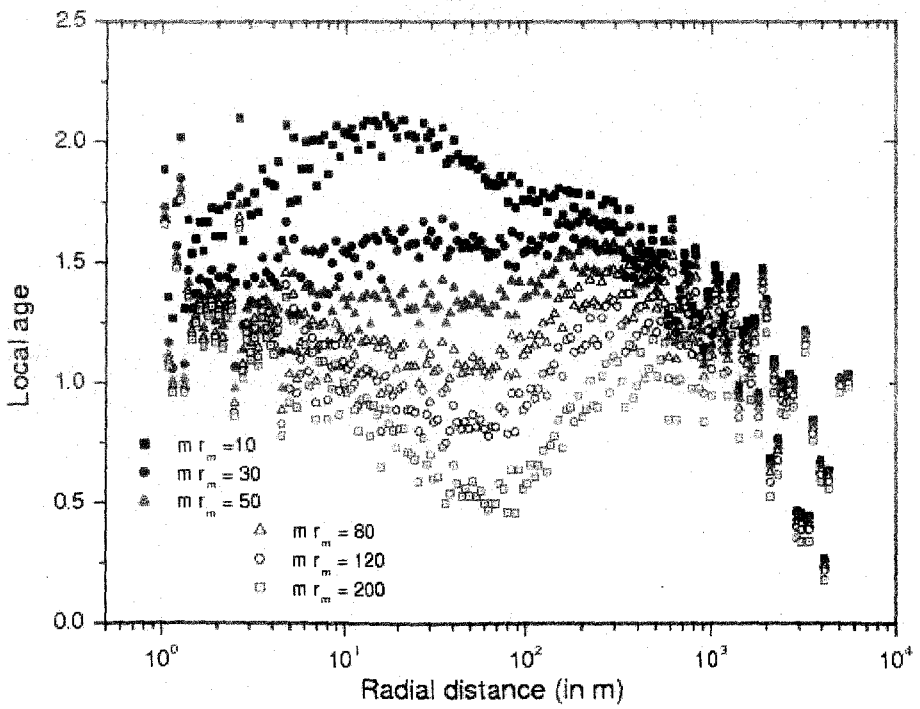
Local age
Radial distance (in m)
m r_m =10
m r_m = 30
m r_m = 50
m r_m = 80
m r_m = 120
m r_m = 200

(b)

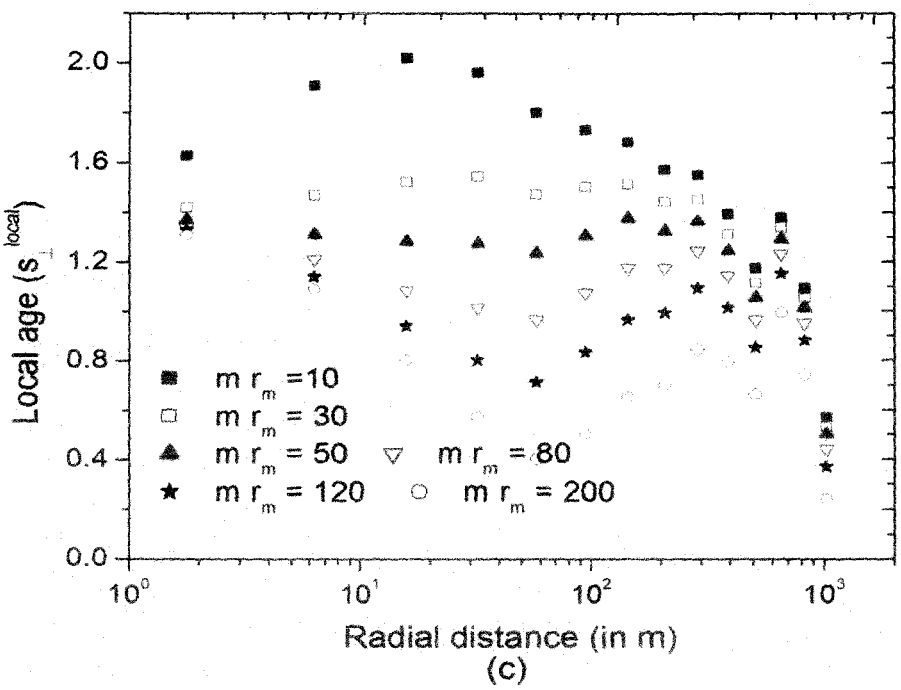

Fig.3.4: Variation of the LAP (estimated from the simulation data) with the radial distance for different choices of the effective Moliére radius at the KASCADE site (a) for proton; (b) for iron with a primary energy 5×10^{17} eV and (c) for γ with a primary energy 10^{15} eV.

To examine systematically the influence of the effective Moliére radius on the shape of the lateral distribution of charged particles in EAS, we study the radial variation of the LAP for different effective Moliére radii, which are shown in **Figs. 3.4a** and **3.4b** for proton and iron primaries with a primary energy of 5×10^{17} eV.

A string-like feature emerged with two nodes, as seen from the figures, one close to the shower core while the other at around $r \sim 400$ m that increases slowly with the effective Moliére radius; the effective Moliére radius behaves somewhat like the tension in a piece of string. Beyond the second node, however, the LAP is found to decrease monotonically with an increase of the radial distance, irrespective of the choice of the effective Moliére radius.

In order to explore the inherent cause of such a feature of the LDD of electrons in hadron initiated EAS, we studied the radial variation of the local age for γ-ray initiated showers, and one such plot at the primary energy 10^{15} eV is shown in **Fig.3.4c**. We found the similar nature of radial variation of the LAP as in the hadron initiated showers. As ascertained in previous simulations (Capdevielle

& Gawin 1982, Bourdeau et al. 1980 & Capdevielle et al. 1990), the behaviour of $s_{\perp}^{local}(r)$ comes mainly from the discrepancies between the EGS4 output and the NKG function, i.e. between the rigorous descriptions of the electromagnetic cascade adopting the basic electromagnetic processes as well as the Moller, Bhaba scattering and positron annihilation, dependence of the cross section on energy on the one hand, *Approximation B* combined with Landau and small angle approximations in a single description of the multiple Coulomb scattering on the other hand. When the experimental data (Antoni et al. 2001, Capdevielle & Cohen 2006[a], 2006[b]) are superimposed on **Fig.3.4**, we understand that a reduced Moliére radius (between 20 - 50 m) is favoured for all primary energies, implying a dramatic reduction in the mean scattering angle connected with the scattering energy of 21 MeV. For primary energies lower than 10^{17} eV, it looks easy to fit the lateral distributions in the range 20 - 100 m and determine the minimum value of $s_{\perp}^{local}(r)$ from the measured densities, as well as its average value over a selected radial distance range. They are representative estimators and a correspondence with $s_{\parallel}$ can be tabulated via adjustments and simulation; at ultra high energy, the detectors are saturated near the core and we suggest a fit of $s_{\perp}^{local}(r)$ around the distances selected for the energy estimator, usually 500, 600, 800 or 1000 m.

3.5 CHARACTERISTICS OF THE SHOWER AGE PARAMETER

To explore the physical nature associated with the lateral shower age parameter, if any, we studied the details of the characteristics of the shower age. For the local age, we considered two different parameters: the minimum value corresponds to the local age at the radial distance, about 50 m, and an average value nearly between 50 to 300 m. Besides, we have taken the NKG lateral age obtained from fitting the density data up to about 100 m.

3.5.1 DISTRIBUTION OF SHOWER AGE PARAMETER

The distributions of the LAP and the lateral shower age were studied for the primary energy range 3×10^{14} to 3×10^{16} eV. Those distributions (for instance **Fig.3.5e**) differ from a Gaussian distribution when the observational level is deeper than the depth of the shower maximum and is found to fit well by an *Extreme Value Distribution* (EVD) defined through

$$\varphi(s) = \frac{1}{\sigma}\exp\left(\pm\frac{\mu - s}{\sigma} - e^{\pm\frac{(\mu-s)}{\sigma}}\right) \qquad (3.10)$$

, where the parameters μ and σ are related to the average size $< s >$ and its variance V_s by $< s > = \mu \pm 0.577\sigma$ and $V_s = 1.645\sigma^2$ (in the case of the histogram of **Fig.3.5f**, $< s > = 1.495$ and $\sigma = 0.07$).

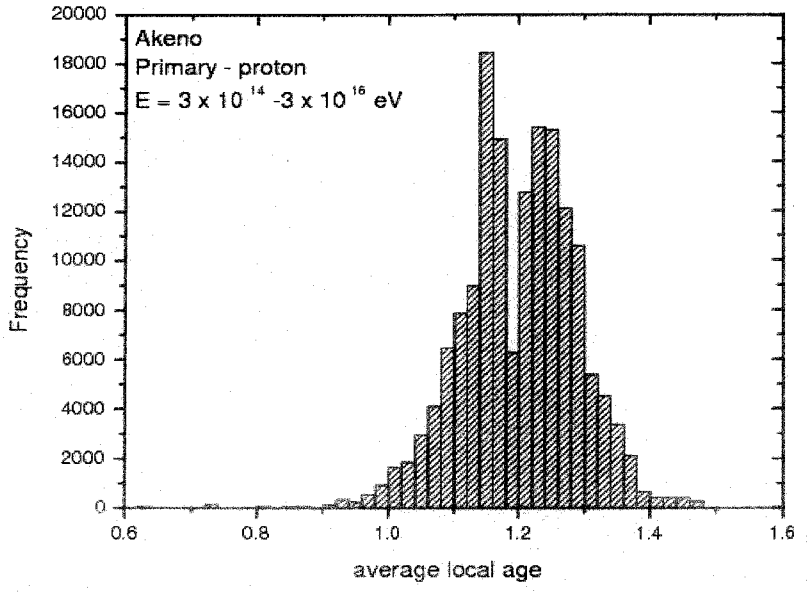

(a)

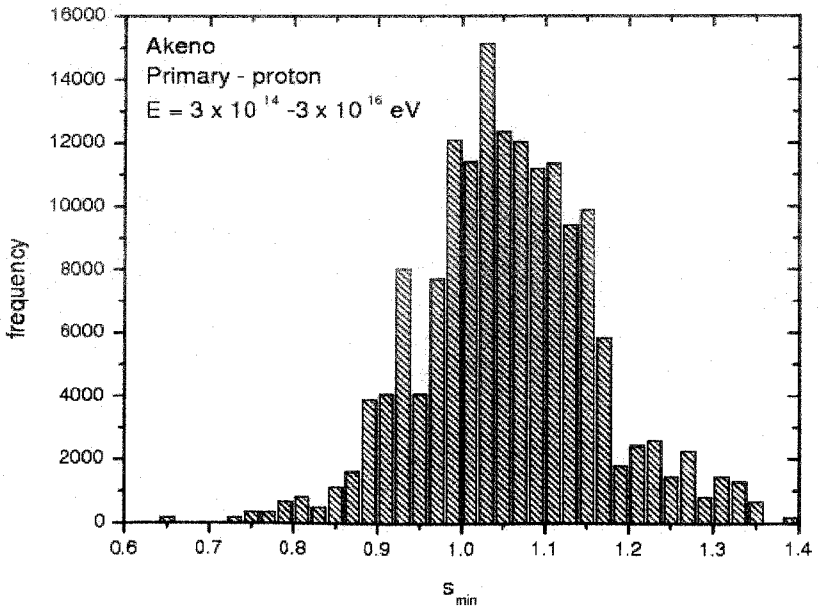

(b)

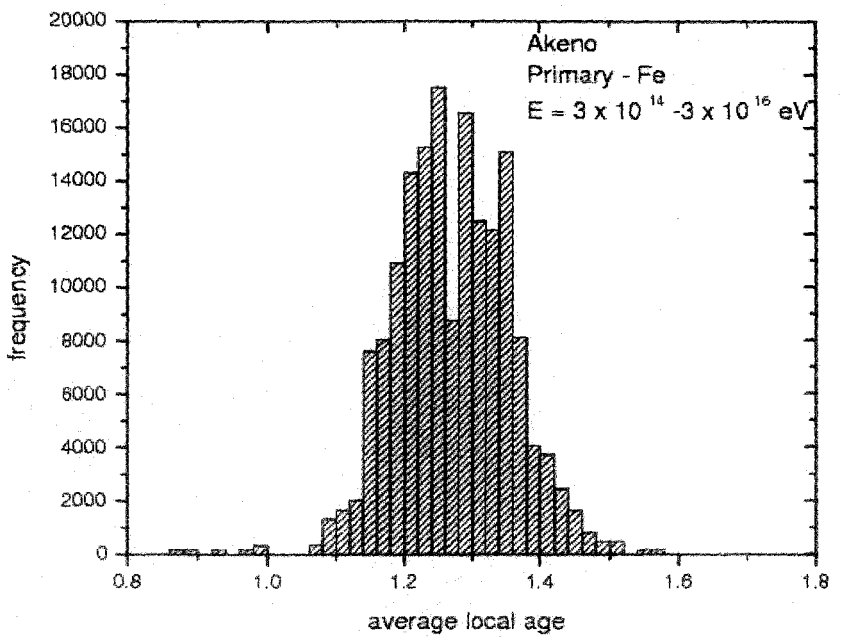
Akeno
Primary - Fe
E = 3 x 10 14 -3 x 10 16 eV
frequency
average local age
0
2000
4000
6000
8000
10000
12000
14000
16000
18000
20000
0.8
1.0
1.2
1.4
1.6
1.8

(c)

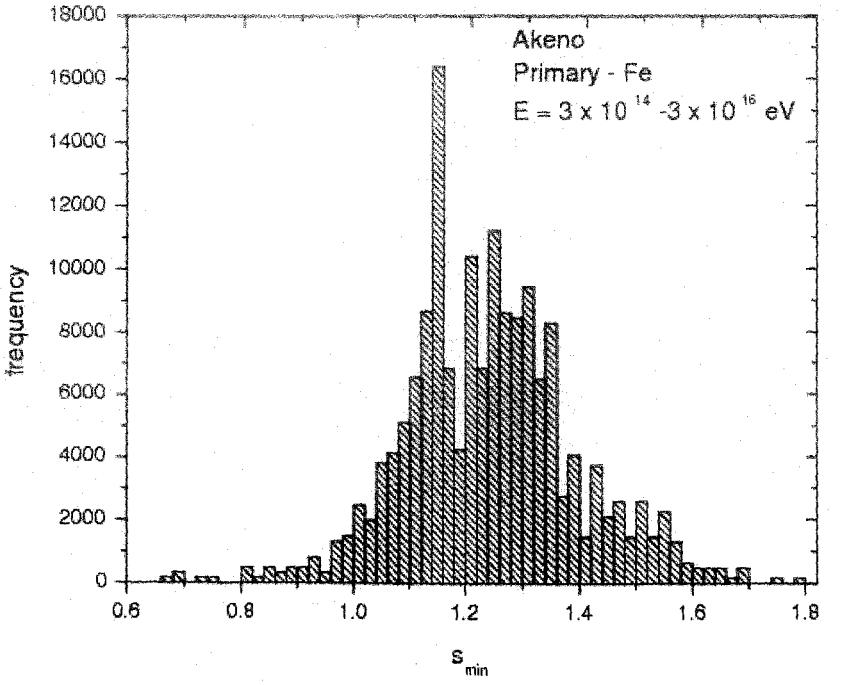
Akeno
Primary - Fe
E = 3 x 10 14 -3 x 10 16 eV
frequency
s min
0
2000
4000
6000
8000
10000
12000
14000
16000
18000
0.6
0.8
1.0
1.2
1.4
1.6
1.8

(d)

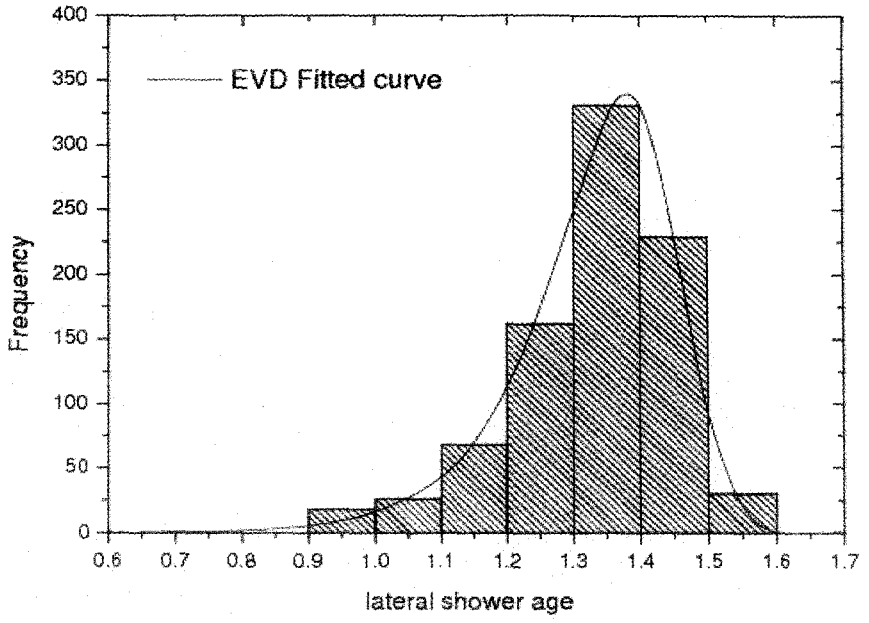
EVD Fitted curve
Frequency
lateral shower age
0
50
100
150
200
250
300
350
400
0.6
0.7
0.8
0.9
1.0
1.1
1.2
1.3
1.4
1.5
1.6
1.7

(e)

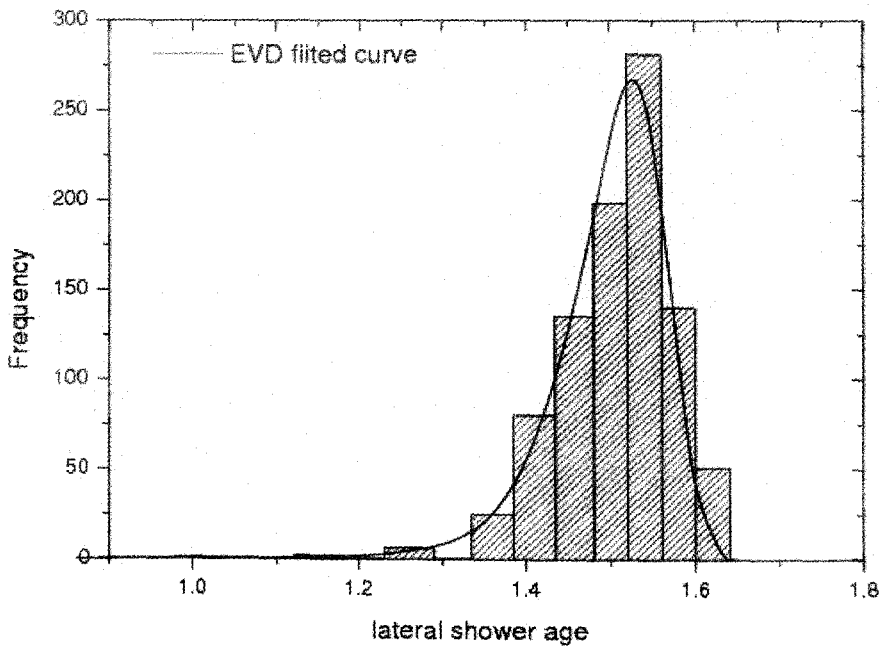
EVD fiited curve
Frequency
lateral shower age
0
50
100
150
200
250
300
1.0
1.2
1.4
1.6
1.8

(f)

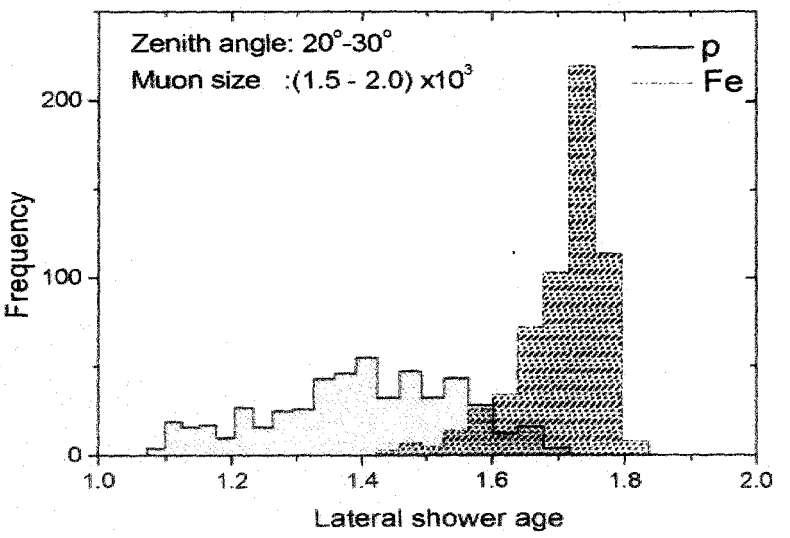

(g)

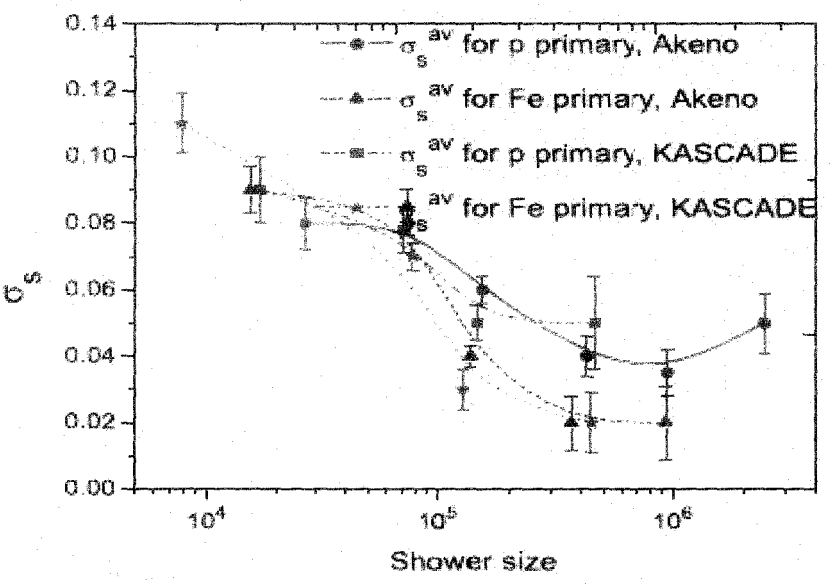

(h)

Fig.3.5: Distribution of age parameter from simulated data: (a) average local age (s_{av}) at Akeno for p primary, (b) minimum local age (s_{min}) at Akeno for p primary, (c) average local age (s_{av}) at Akeno for Fe primary, (d) minimum local age (s_{min}) at Akeno for Fe primary; (e) NKG-fitted lateral age at sea level for p primary, (f) NKG-fitted lateral age at sea level for Fe primary, (g) NKG-fitted lateral age at sea level for p and Fe primaries within a small muon window. (h) The variance (σ) of the LAP as a function of shower size. The lines are only a guide for the eye.

The fluctuations in lateral shower age are much larger for proton initiated showers in compared to those initiated by heavier primary as revealed from the **Fig.3.5**. This is clear on **Fig.3.5e** and **Fig.3.5f** where the frequencies reflect the intensities of primaries around the knee. The long tail in the left wing of **Fig.3.5f** corresponds to very penetrating proton showers of low primary energy and conversely the steep right wing contains showers interacting at very high altitude whereas the central part is populated by showers with an individual maximum close from average maximum at each energy.

Similar features concern the case of the pure iron component (see **Fig.3.5f**) with a general reduction of r.m.s. of the fluctuation. If we consider a small primary energy bin instead of a wide one, for instance by selecting the showers inside a small muon size band, we observed that both the distributions of p and Fe could be separated, which in fact becomes very contrasted as shown in **Fig.3.5g**; this approach, if adopted with the experimental data, may yield important information on the primary composition around the knee region.

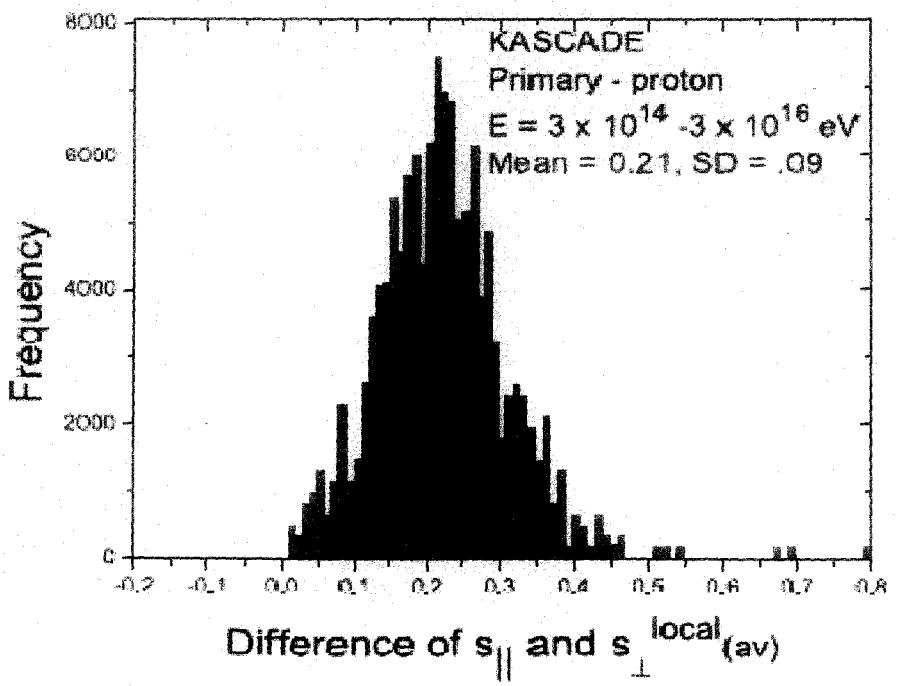

(a)

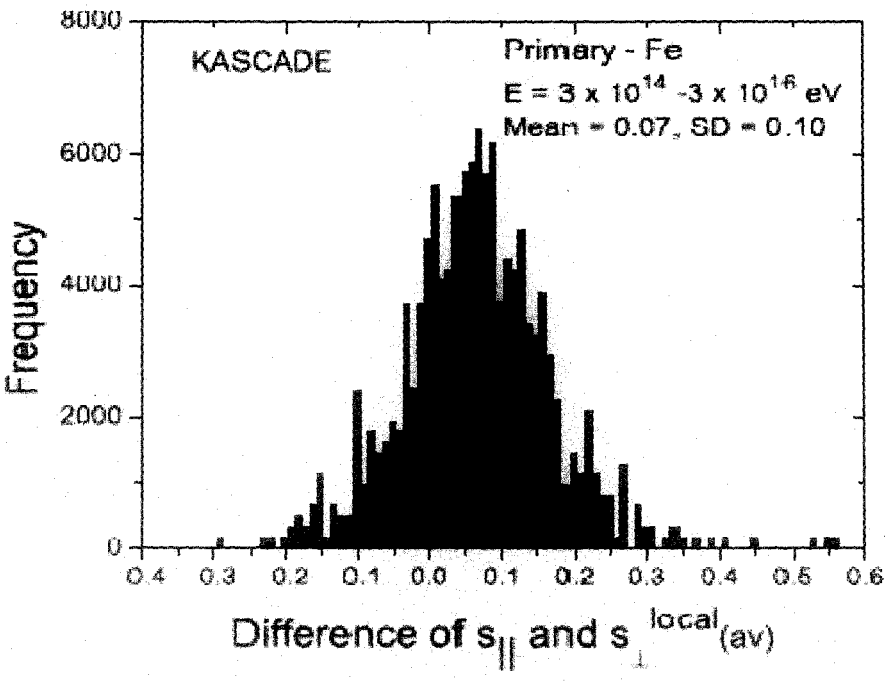
KASCADE
Primary - Fe
E = 3 x 10^14 -3 x 10^16 eV
Mean = 0.07, SD = 0.10
Frequency
8000
6000
4000
2000
0
0.4 0.3 0.2 0.1 0.0 0.1 0.2 0.3 0.4 0.5 0.6
Difference of s|| and s⊥ local(av)

(b)

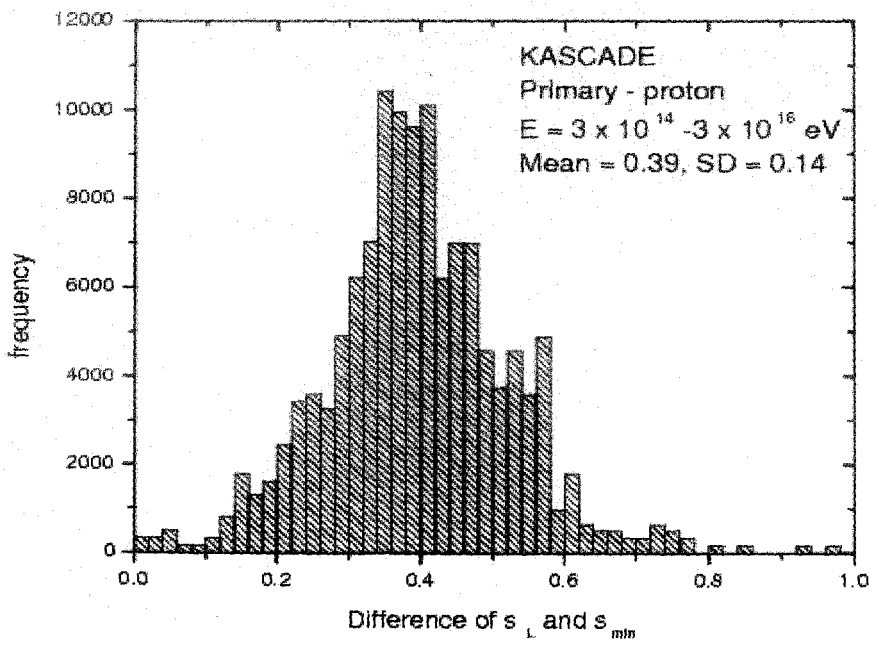
KASCADE
Primary - proton
E = 3 x 10^14 -3 x 10^16 eV
Mean = 0.39, SD = 0.14
frequency
12000
10000
8000
6000
4000
2000
0
0.0 0.2 0.4 0.6 0.8 1.0
Difference of s⊥ and smin

(c)

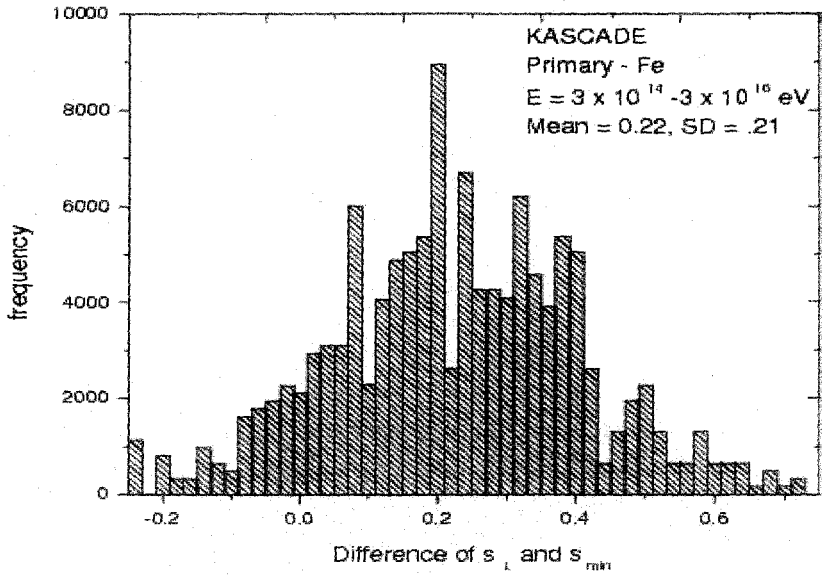

(d)

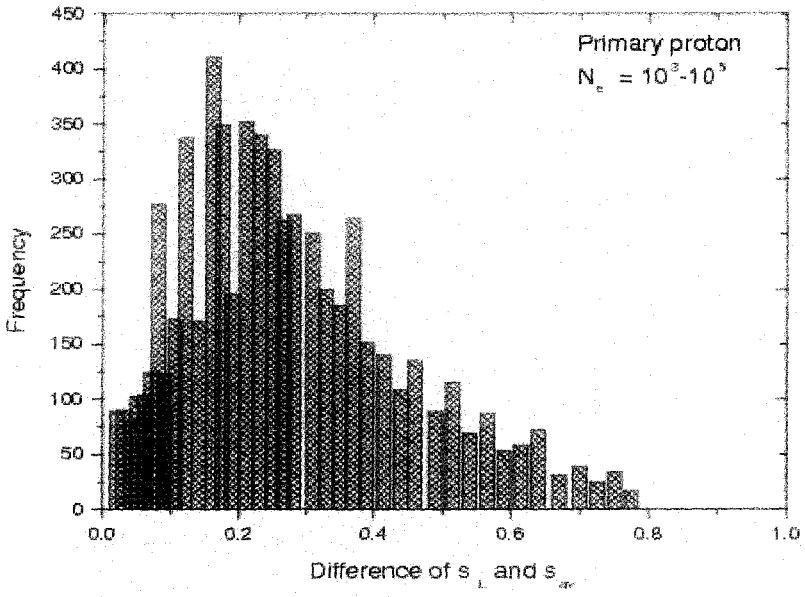

(e)

Fig.3.6: Distribution of the difference between the longitudinal shower age and average local age/minimum local age or NKG-fitted shower age from simulated data. KASCADE: $(s_{\parallel} - s_{\perp}^{local}(av))$ **(a)** p and **(b)** Fe; KASCADE: $(s_{\parallel} - s_{min})$ **(c)** p and **(d)** Fe: KASCADE: $(s_{\parallel}\text{-}\ s_{\perp}(av))$ **(e)** p.

3.5.2 THE FLUCTUATION OF SHOWER AGE PARAMETER

The fluctuations (σ) i.e. variances in the LAP in different shower age bins are estimated and as a function of the shower size are drawn in **Fig.3.5h** for proton and iron primaries for the interaction model QGSJET. In accordance with experiments (Catz et al. 1973), the fluctuations in the LAP were found to be larger for the proton initiated showers in comparison to those initiated by the primary iron, except at lower energies. Similar trends have been found from simulated data when the lateral age parameter and its fluctuation were in use (Dey et al. 2011).

3.5.3 LONGITUDINAL AGE VERSUS LATERAL AGE

For each simulated event the longitudinal shower age has also been estimated exploiting the relation (**3.9**) (or directly obtained longitudinal age delivered by the output of the NKG option of CORSIKA) and the difference between the two age parameters, longitudinal age ($s_{\parallel}$) and average local age $s_{\perp}^{local}(av)$ or NKG fitted lateral age ($s_{\perp}$) is obtained. A frequency distribution of a number of differences between two age parameters at KASCADE site is given in **Fig.3.6**.

The frequency distributions of the differences between two age parameters ($s_{\parallel}$) and $s_{\perp}^{local}(av)$) for proton and Fe primaries are given in **Figs.3.6a – 3.6b**. The frequency distributions of the differences between two age parameters ($s_{\parallel}$ and s_{min}) for proton and Fe primaries are given in **Figs.3.6c – 3.6d**. From **Figs. 3.6a** and **3.6b**, it is clear that the frequency distribution for proton primary exhibits peak, at around 0.2, is consistent with the early observations (Capdevielle & Gawin 1982, Bourdeau et al. 1980, Capdevielle et al. 1990, Dedenko et al. 1975 & Stamenov 1987), whereas for Fe initiated showers the peak difference is much lower, at about 0.07. However, for a non-negligible fraction of events, the differences between the two shower age parameters were found to be substantial. The same study has been made using simulated data at Akeno site for proton and iron primaries in the concerned energy range and the distributions are shown in **Figs.3.7a – 3.7d**.

For the EGS4 data at 10^{18} eV at Akeno site we estimated the average local age between 50 m to the radius of shower disk as may be revealed to an EAS array equipped with particle detectors of area ~ 1 m^2 and found that such an average age is very close to the longitudinal age.

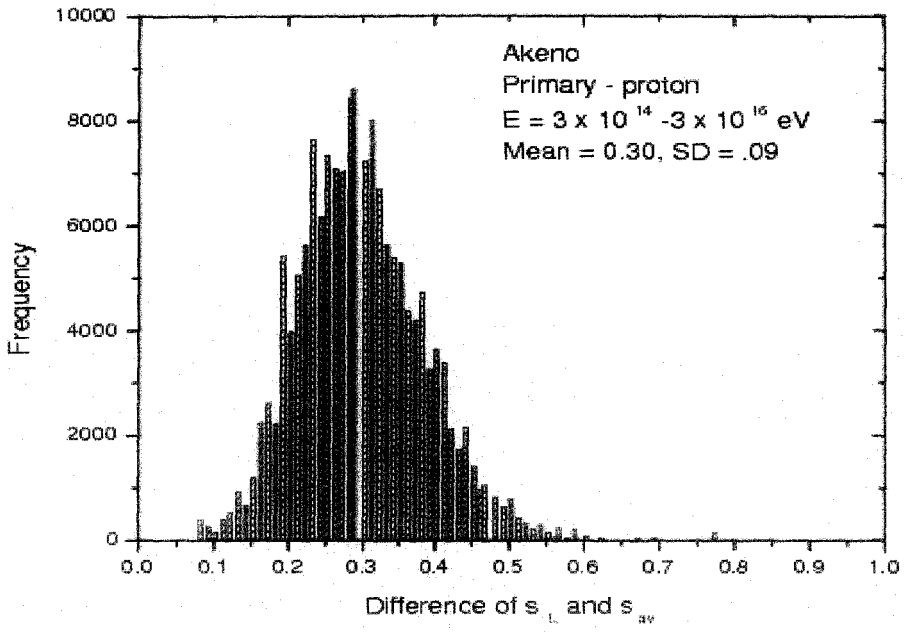
Akeno
Primary - proton
E = 3 x 10 14 -3 x 10 16 eV
Mean = 0.30, SD = .09
Frequency
Difference of s L and s av
10000
8000
6000
4000
2000
0
0.0
0.1
0.2
0.3
0.4
0.5
0.6
0.7
0.8
0.9
1.0

(a)

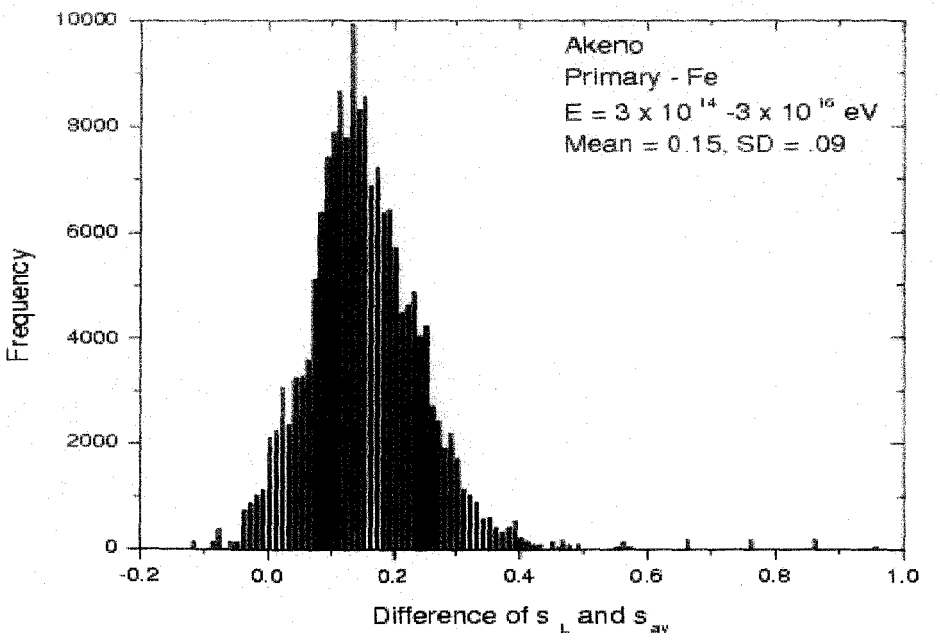
Akeno
Primary - Fe
E = 3 x 10 14 -3 x 10 16 eV
Mean = 0.15, SD = .09
Frequency
Difference of s L and s av
10000
8000
6000
4000
2000
0
-0.2
0.0
0.2
0.4
0.6
0.8
1.0

(b)

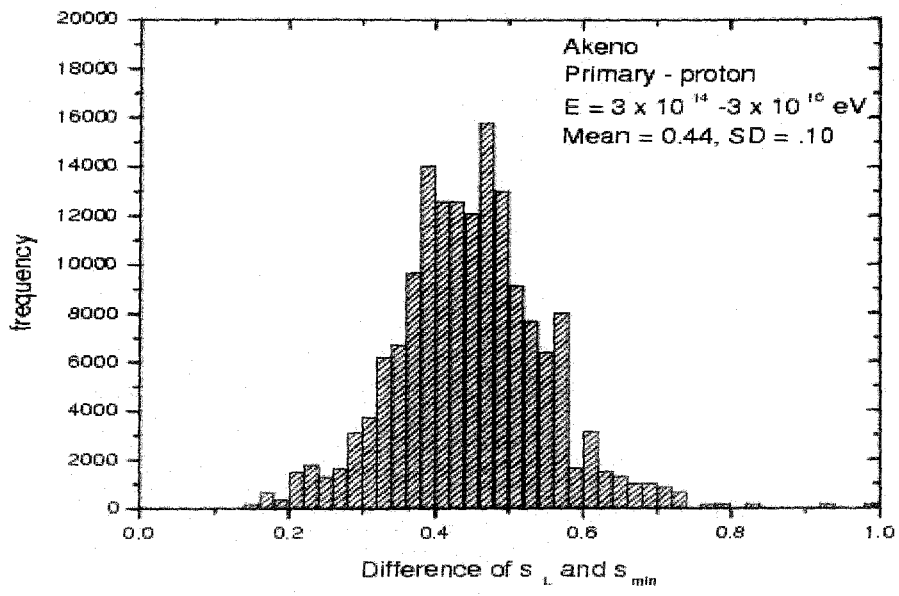

(c)

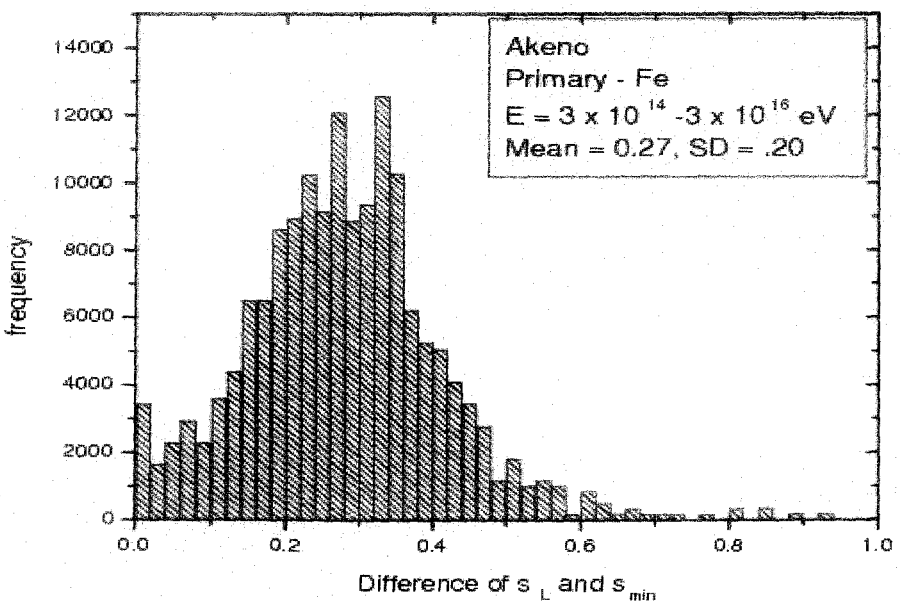

(d)

Fig.3.7: Distribution of the difference between the longitudinal shower age and average local age/minimum local age from simulated data. Akeno: $(s_{\parallel} - s_{\perp}^{local}(av))$ **(a)** p and **(b)** Fe; Akeno: $(s_{\parallel} - s_{min})$ **(c)** p and **(d)** Fe.

3.6 THE CORRELATION OF SHOWER AGE PARAMETER WITH OTHER EAS OBSERVABLES

3.6.1 VARIATION OF LATERAL SHOWER AGE WITH ATMOSPHERIC DEPTH

With the increase of zenith angle a shower traverses an increased thickness of atmosphere which immediately suggests that the EAS with higher zenith angle should be older in shower age than the EAS of smaller zenith angle but of same primary energy. Based on this idea we have studied variation of lateral shower age with atmospheric depth from the simulated data.

The **Fig.3.8a** shows the lateral shower age as a function of $\sec(z)$ for two primary energy intervals at NBU site. Separate samples of proton and Fe initiated showers are considered to investigate the said aspect. The variation of local shower age with atmospheric depth has also been studied for fixed primary energy range which is shown in **Fig.3.8b**. In **Fig.3.8c**, we plot the same variation but for muon size intervals at KASCADE site.

It is seen from the **Fig.3.8** that for both proton and Fe initiated showers the local/lateral shower age monotonically increases with atmospheric depth reflecting a strong correlation of the parameter with longitudinal development.

In order to check the influence of the hadronic interaction models on the results we compare NKG lateral shower age versus atmospheric depth variations for two different models, the QGSJET and the SIBYLL, which is shown in **Fig.3.8a**. The SIBYLL gives comparatively higher value of lateral shower age but the nature of dependence of lateral shower age on atmospheric depth is found similar in both the two hadronic interaction models. This discrepancy may come from the cross section for p-air collisions rising more rapidly versus energy in SYBILL than in QGSJET.

The present simulation study suggests that the lateral shower age/local age can be expressed as a function of zenith angle by the empirical relation

$$s_{\perp} = s_0 + A \sec(z) \qquad (3.11)$$

The value of s_0 and A for different shower size ranges can be obtained by fitting the simulated data generated with either QGSJET or SIBYLL.

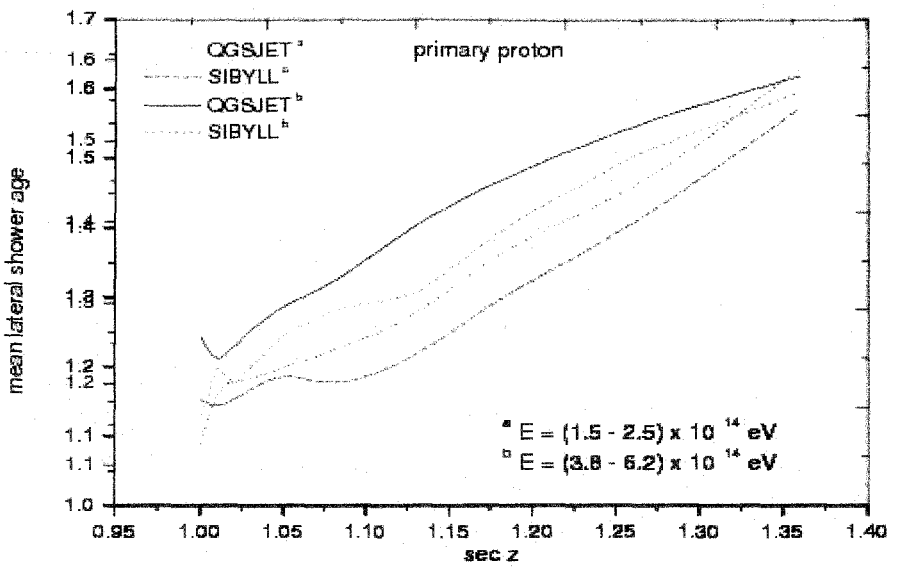

(a)

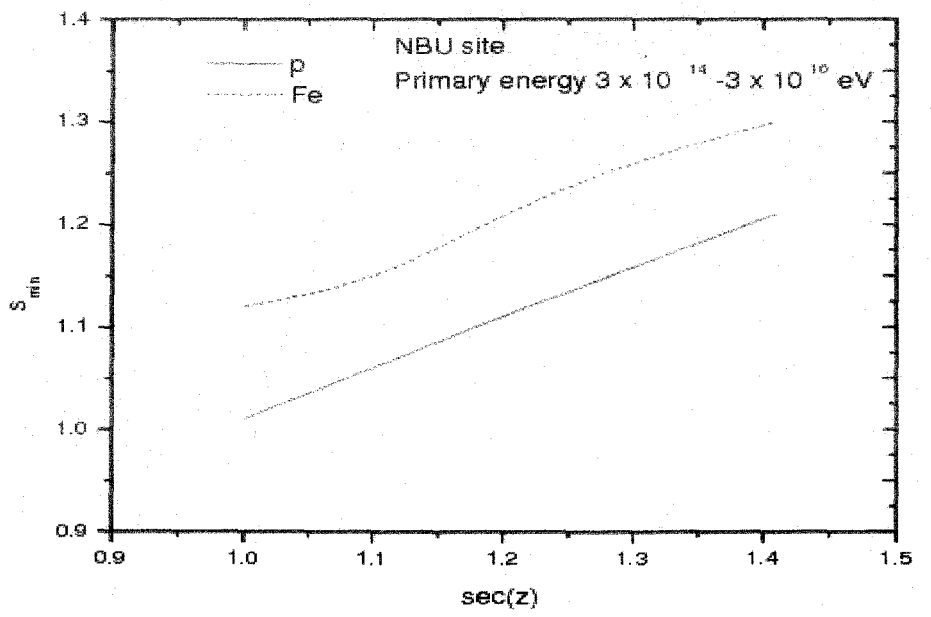

(b)

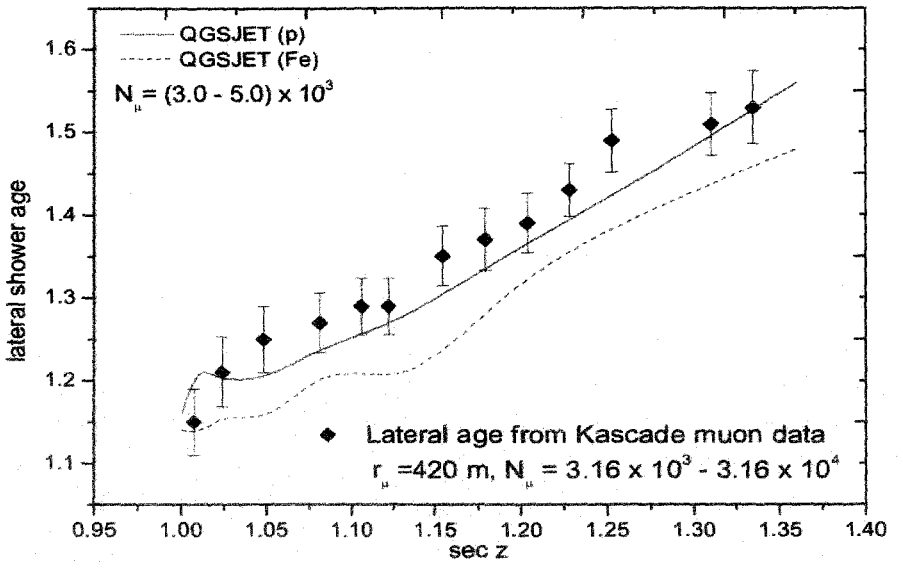

(c)

Fig.3.8: Variation of shower age with atmospheric depth (a) lateral shower age at NBU site for two fixed primary energy intervals and hadronic models, (b) minimum local age at NBU site for a fixed primary energy range and (c) lateral shower age at KASCADE site for a fixed muon size interval along with lateral shower age from KASCADE observed muon lateral distribution data.

Equation (**3.11**) can be written as $s_{\perp} = s_0 + A\frac{x}{x_v}$, where x and x_v are the atmospheric thickness travelled by the EAS and vertical atmosphere depth respectively. It thus immediately follows $\frac{ds_{\perp}}{dx} = \frac{A}{x_v}$. The change of lateral shower age over an atmospheric depth of 100 gm-cm^2 for the simulated data generated with QGSJET lies within $(2 - 4)\times 10^{-2}$ corresponding to the shower size range $10^3 - 10^4$.

3.6.2 VARIATION OF LATERAL SHOWER AGE WITH ELECTRON SIZE

The variation of the local shower age at a radial distance of about 50 m (minimum value) or mean lateral shower age (NKG-fitted) with average shower size, obtained from the simulated results for both proton and iron primaries at the Akeno, KASCADE and NBU locations are presented in **Figs. 3.9a - 3.9c**. The corresponding observational results extracted from the Akeno and KASCADE experimental data are also shown in **Fig.3.9a** and **Fig.3.9b**. For Akeno

experimental data, we extracted a minimum local age for the different shower sizes from reference (Nagano et al. 1984[b]), whereas for KASCADE we estimated it from their measured lateral distribution (Antoni et al. 2001, Apel et al. 2006, Ulrich et al. 2008 & 2009[a]). We note here that being a small EAS array, the radial density measured by the NBU EAS array was restricted to much smaller core distances in compared to the KASCADE or Akeno experiments. As a result shower size estimated by the array, particularly at higher energies corresponding to large electron sizes, may have considerable uncertainties and hence resolving power of the array in respect to primary mass composition is expected to be limited. On the other hand, in the KASCADE or Akeno measurements shower size is basically estimated through NKG fitting considering particle densities up to a larger core distance for EAS with higher primary energies. In view of the radial variation of lateral age such a procedure of estimating shower size may involve some bias on the estimated shower size though the magnitude of such systematic error is not large.

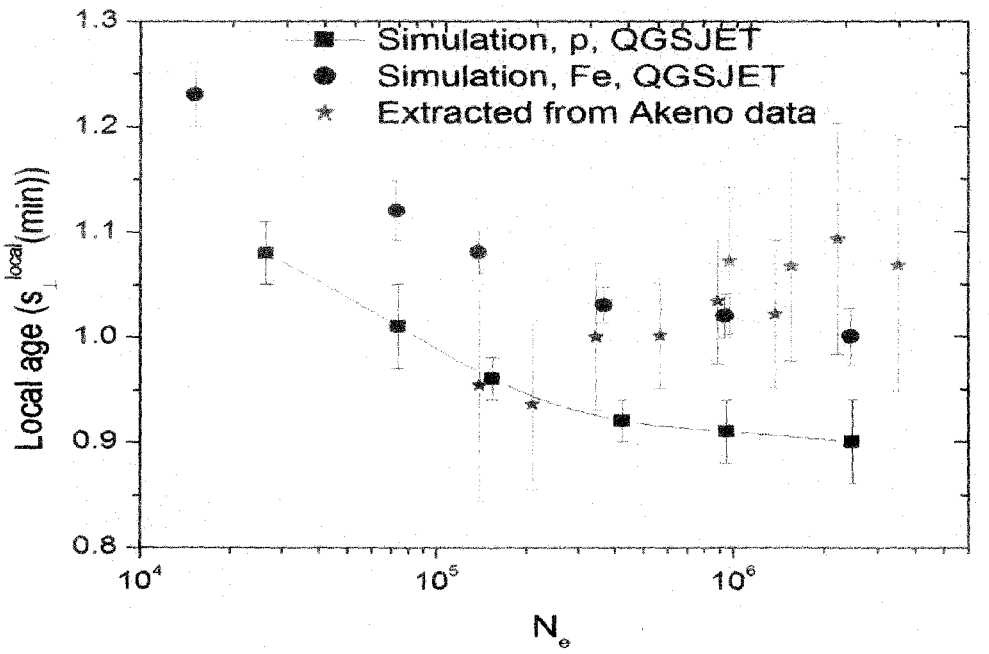

(a)

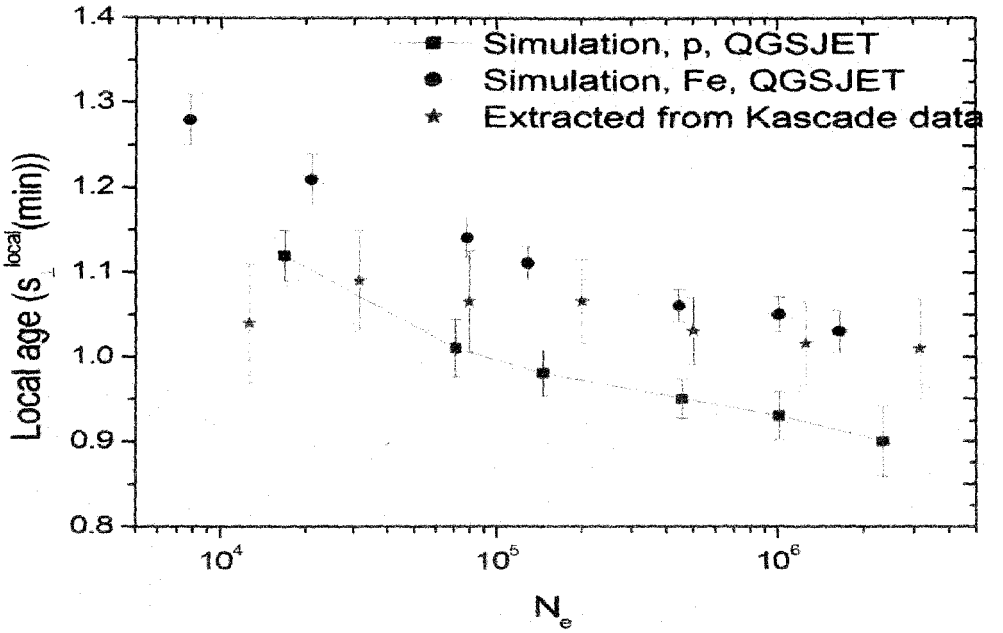

(b)

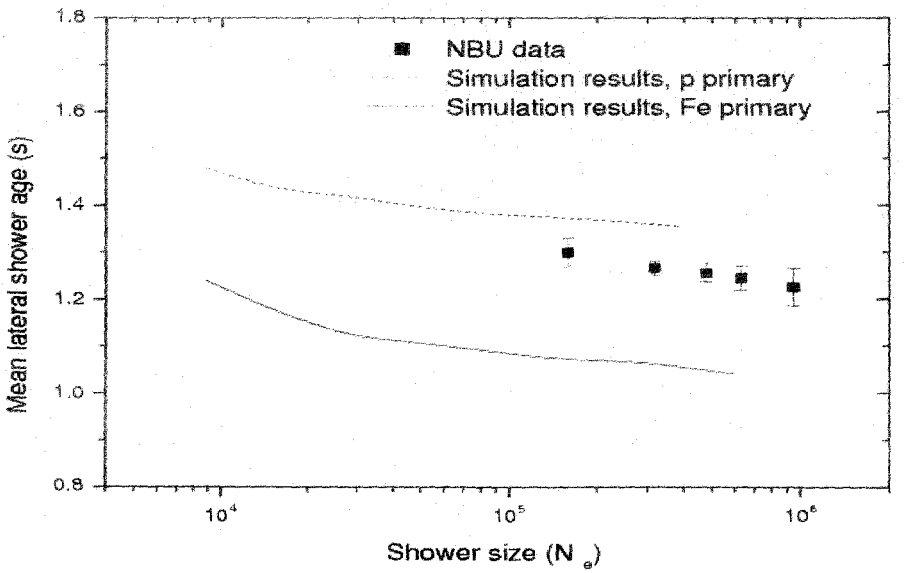

(c)

Fig.3.9: Variation of the lateral shower age with electron size for proton and Fe primaries at (a) Akeno, (b) KASCADE and (c) NBU locations. For KASCADE and Akeno data the estimated minimum value of the local age is used while for NBU data the lateral age is estimated through the traditional shower reconstruction method.

It is noticed from the figures that the local or lateral shower age decreases with shower size but the rate of decrease slows down at higher shower size. With increasing primary energy i.e. with increasing shower size showers penetrate deeper into the atmosphere resulting in steeper lateral distribution indicated by the smaller lateral shower age parameter (Apel et al. 2006). The simulation results show that showers induced by heavier primaries are older compared to those generated by light primaries. The similarity found in the variation of shower age with shower size for two hadronic interaction models QGSJET and SIBYLL indicates that the longitudinal development of the electromagnetic component is alike in both the models.

The comparison of the simulated results with the experimental observations from both the Akeno and KASCADE EAS experiments (**Figs. 3.9a** and **3.9b**) indicate a need for a change in the primary composition towards a heavier primary, as the energy increases across the *knee* of the primary energy spectrum. The KASCADE group also reached a similar conclusion using the shape parameter instead of the shower age (Apel et al. 2006), as well as from the study of the muon content in EAS (Antoni et al. 2002). The present data of the LHC, especially the pseudo-rapidity density distributions, suggest larger multiplicities and inelasticities than in the models used in the CORSIKA simulations (Capdevielle 2010). However, up to energy of 2.6×10^7 GeV, this could result in a very small reduction of the reported enhancement of the primary mass with energy.

3.6.3 VARIATION OF THE LATERAL SHOWER AGE WITH MUON SIZE

The variation of local/lateral shower age with muon size has also been studied for the zenith angle range 0^0 - 45^0 for both proton and iron primaries and are plotted in **Fig.3.10a** and **3.10b** at Akeno, and KASCADE levels. The variation exhibits the same nature as obtained in the KASCADE experiment using NKG fitting for muons with slightly higher threshold energy (Antoni et al. 2001). With increasing primary energy i.e. with increasing muon size showers penetrate deeper into the atmosphere resulting in steeper lateral distribution indicated by the smaller lateral shower age parameter (Apel et al. 2006). The simulation results show that showers induced by heavier primaries are older compared to those generated by light primaries. The similarity found in the variation of shower age with muon size for two models QGSJET and SIBYLL revealing once again that the longitudinal development of the electro-magnetic component is independent of the hadronic interaction models.

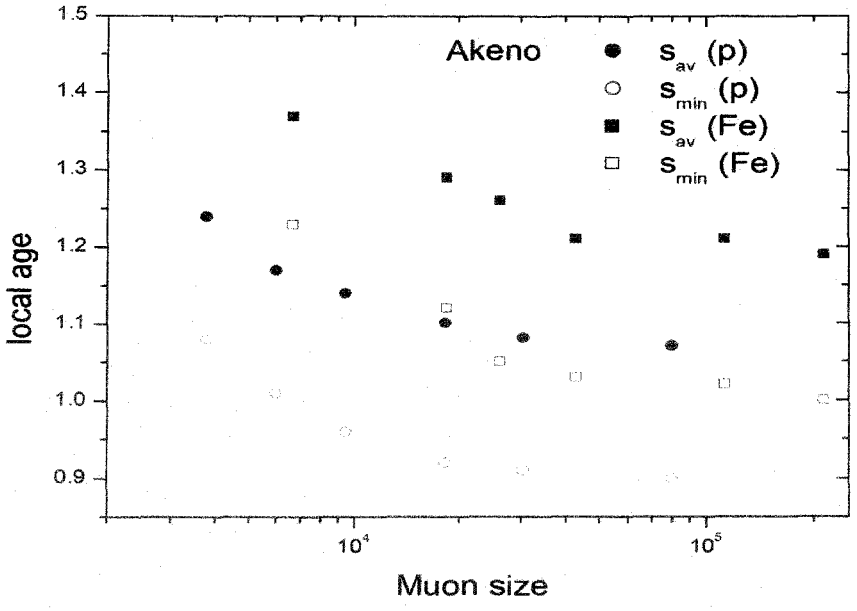

(a)

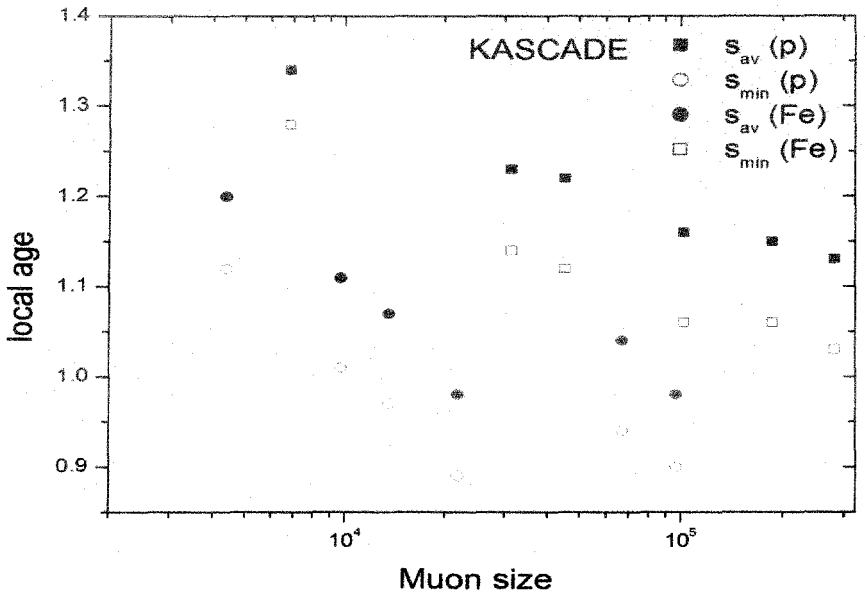

(b)

Fig.3.10: Variation of average/minimum value of the local age with muon size for p and Fe (a) at Akeno and (b) at KASCADE locations.

3.6.4 THREE DIMENSIONAL VARIATION OF N_e, N_μ and s

Muon content of EAS generally used to extract information on the composition of cosmic ray primaries. However, as mentioned earlier due to uncertainties in the interaction model and the difficulties associated with the solutions to the EAS inverse problem, separating the primary energy spectra of elemental groups remains ambiguous. Iron and proton initiated showers may be better separated employing shower age and muon content simultaneously through 3-dimensional plot of shower size and shower age than in either of its 1-dimensional projections. It is also found that accuracy of determining the nature of primary species increases with the simultaneous use of shower age and muon content.

In **Fig.3.11** we plot the 3-dimensional curve between average local shower age at a radial distance about 50 m (minimum value), average shower size and muon size obtained from simulation results for both proton and iron primaries at Akeno and KASCADE levels. The corresponding observational results of the Akeno and KASCADE experiments are also given in the figures. For the Akeno experimental data we extract the minimum local age for different shower sizes from (Nagano et al. 1984[b]) whereas the mean muon content corresponding to those shower sizes are obtained from reference (Dixon & Turver 1974). In the case of KASCADE data, we estimated local age from their measured lateral distribution (Antoni et al. 2001, Ulrich et al. 2008 & 2009[a]) and corresponding muon size are extracted from the $N_e - N_\mu$ curve (Werner et al 2006, Pierog & Werner 2008[a]).

The comparison of simulated results with experimental observation from both the Akeno and KASCADE EAS experiments indicate for a change in primary composition towards heavier primary as energy increases across the *knee* of the primary energy spectrum. The KASCADE group also reached the same conclusion using slope parameter instead of shower age.

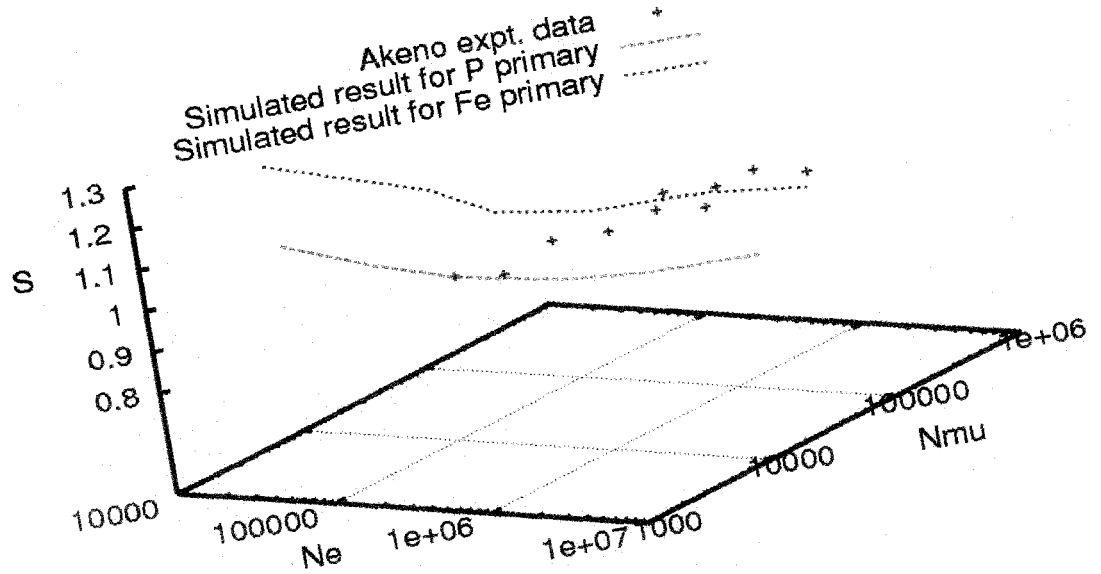

(a)

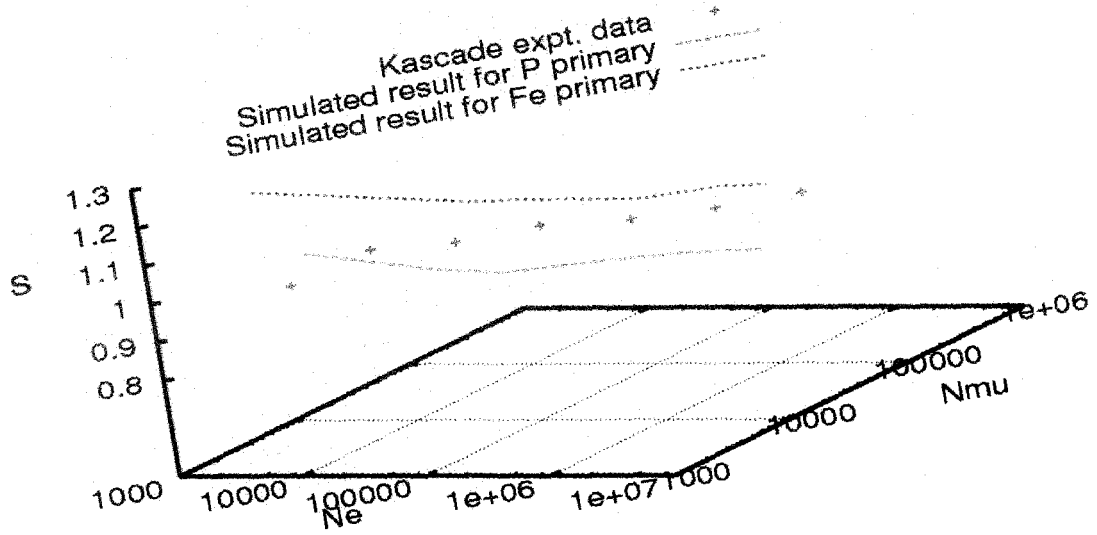

(b)

Fig.3.11: 3-Dimensional plot between shower size, muon size and mean local shower age for proton and Fe primaries at (a) Akeno and (b) KASCADE locations.

3.7 CONCLUSIONS

From the present analysis we conclude the following:

1. The lateral distribution of electrons in EAS exhibits some sort of *scaling* (energy independent) behaviour in terms of the local age. The characteristic feature of the local age versus the radial distance curve is that with an increase of the radial distance, the local age decreases initially and reaches a minimum at around 50 m then it starts increasing, attaining local maxima at around $300-400$ m, and then starts decreasing again. Such a feature appears to be independent of the energy of the EAS initiating particle, at least there is no strong dependence on the primary energy. Such a characteristic radial variation in the local age is found as a generic feature of electromagnetic cascades.
2. The local age offers a good solution towards an unambiguous estimation of the shower age. Since the shower age varies with the radial distance, even for the modified NKG functions, a comparison of the lateral shower age of different EAS experiments is not meaningful, as the radii of the shower discs naturally differ from experiment to experiment, depending on the experimental set up. Even in a single EAS experiment different events have different radial extensions and thus a lateral age obtained through fitting with the NKG function seems ambiguous. The local age at a particular distance (say at about 50 m where it takes the minimum value) is, however, not always practical owing to the large fluctuation in the electron density data in a real measurement. A rational idea could be to take some sort of average local age between the first minimum, at around a core distance of 50 m, and the subsequent local maximum, at around 300 meter. Experimentally the radial variation of the LAP can be checked properly with a full coverage detector array, like ARGO-YBJ (Pierog & Werner 2008[b]). Note that at smaller distances before the first minimum the detectors of EAS experiments often exhibit saturation effect leading ambiguous electron densities at that region.
3. Use of a modified NKG function or more specially employing a reduced Moliére radius in NKG function leads to a constant shower age over a radial distance up to about 350 m but the magnitude of shower age estimated in such a manner is found to be quite higher in comparison with that of

longitudinal age. But even with such reduced Moliére radius, local age is found to decrease sharply after say about 400 m.

From the study of local age in gamma ray initiated showers, it is found that the parameter varies with radial distance and the radial variation of the parameter is alike to what we observe in the case of hadron initiated showers. Which implies that the radial variation of local age in hadron initiated showers is not due to superposition of several gamma ray induced showers but it further reveals the generic feature of pure electromagnetic cascades.

4. The lateral age offers a good estimator of the longitudinal development of an EAS cascade, as already noted in some earlier works (Capdevielle & Gawin 1982, Bourdeau et al. 1980, Capdevielle et al. 1990, Stamenov 1987, Dixon & Turver 1974). However, the parameter correlates with the stage of the shower development on a statistical basis; the average of this parameter increases as air showers traverse an increased thickness of atmosphere. The experimental observations (Bhadra 1999) also substantiate such behaviour. The slope of lateral shower age versus atmospheric depth curve is, however, more or less the same for proton and iron initiated showers. The distribution of the differences between the local age and the longitudinal age also indicate the strong correlation between the two ages. Such a feature has been noted for two different hadronic interaction models, the QGSJET and the SIBYLL, and hence appears robust. It is imperative to examine such correlations using EPOS (Werner et al. 2006, Pierog & Werner 2008[a]), the only model that seems to be providing quite a consistent description of the longitudinal and lateral EAS profiles (Pierog & Werner 2008[b]), which would need to be performed in future work.

   The distribution of differences between local or lateral shower age and longitudinal age also indicate the strong correlation between these two ages.

5. The fluctuation of the LAP was found to be sensitive to the nature of the primary particle. However, the level of uncertainty in determining the lateral shower age from the experimental data is comparable with the magnitude of fluctuation and hence deriving any firm conclusion on the nature of the primary only from the shower age fluctuation is difficult. If showers within a small bin of the primary energy could be selected, for instance by considering shower events in a small muon size interval, the distribution of shower age was found to be quite sensitive on primary composition.

6. The local/lateral shower age takes higher value for iron initiated showers in compared to that of proton initiated which means that lateral distribution of electrons for iron initiated EAS is flatter relative to that of proton initiated EAS. This feature is reflected in the variations of shower age with both electron size and muon content independently. The comparison of the simulated results with the Akeno and the KASCADE observations in respect to a variation of the shower age with shower size around the *knee* indicates a change in the primary composition towards heavier primaries across the *knee*. This finding supports the results obtained from the study of the muon content in EAS.
7. For the study of primary composition the 3-*dimensional* plot of shower size versus muon size and shower age seems to offer better accuracy in compare to the more conventional approach of implementing it through the shower size versus muon size curve. It would be an interesting task to apply such 3-*dimensional* plot to obtain the composition of primary cosmic rays using observed EAS data from a closely packed air shower array with the facility of concurrent muon measurements such as the GRAPES experiment at Ooty (Gupta et al. 2005).

APPENDIX A

ELEMENTS ON THE THEORY OF THE ELECTROMAGNETIC CASCADE

The one dimensional (1D) and the three dimensional theories (3D) are distinguished based on whether the theory addresses just longitudinal or both lateral and longitudinal shower development. In the analytic approach the time distribution can be derived from the solution of the 3D model providing the densities of the particles and their energy distributions. The 4D simulation is more generally reserved to the MC approach where electrons and photons are followed simultaneously in space-time coordinates (Heck et al. 1998 & Capdevielle 1992).

A.1 *Approximations in the theoretical model of the cascade diffusions equations*

The *Approximation A* neglects the ionization losses taking into account the radiation process and the pair creation process. It allows establishing from the elementary gains and losses in particles and energy. In the case of the 1D theory the simplest system of transport equations which are perfectly symmetric (Nishimura J 1967) is given by

$$\frac{\delta\pi}{\delta t} = -A'\pi + B'\gamma \qquad (A1)$$

$$\frac{\delta\gamma}{\delta t} = -\sigma_0\gamma + C'\pi \qquad (A2)$$

We use here the notations of Nishimura in (Nishimura 1967), $\pi(E,t)dE$ and $\gamma(E,t)dE$ representing respectively the average numbers of electrons and photons with energy between E and $E+dE$ at a depth t in radiation lengths. The operators A' and B' correspond respectively to the losses in electron number by bremsstrahlung and gains by pair productions, whereas the operators σ_0 and C' describe the gain in number of photons by C'. C' is calculated in the assumption of complete screening.

The *Approximation A* is better adapted to the growing phase of the cascade and to high energy photons and electrons. The *Approximation B* is more realistic one. In addition to the approximations stated under *Approximation A* it also incorporates the effect of the ionization loss $\epsilon\frac{\delta\pi}{\delta t}$, thus the equation (A1) becomes,

$$\frac{\delta\pi}{\delta t} = -A'\pi + B'\gamma + \epsilon\frac{\delta\pi}{\delta E}. \qquad (A3)$$

In parallel, the 3D diffusion equations can be inferred after introducing the functions $\pi(E,r,\theta)$ and $\gamma(E,r,\theta)$. For instance, in the case of the *Approximation B* they take the simple form in the so called Landau approximation:

$$\frac{\delta\pi}{\delta t} + \theta\frac{\delta\pi}{\delta r} = -A'\pi + B'\gamma + \epsilon\frac{\delta\pi}{\delta E} + \frac{E_s^2}{4E^2}\left(\frac{\delta^2\pi}{\delta\theta_1^2} + \frac{\delta^2\pi}{\delta\theta_2^2}\right) \qquad (A4)$$

$$\frac{\delta\gamma}{\delta t} + \theta\frac{\delta\gamma}{\delta r} = -\sigma_0\gamma + C'\pi \qquad (A5)$$

The more general differential description in *Approximation B* without Landau simplification is obtained by replacing in this last system equation (A5) by the expression

$$\frac{\delta\pi}{\delta t} + \theta\frac{\delta\pi}{\delta r} = -A'\pi + B'\gamma + \epsilon\frac{\delta\pi}{\delta E} + \int[\pi(\theta-\theta') - \pi(\theta')]\sigma(\theta')d\theta' \qquad (A6)$$

The multiple Coulomb scattering governs the lateral deflections submitted by the electrons passing through the atmosphere. The small angle approximation owing a simple expression of the mean scattering angle when the electron passes through an elementary thickness dt is an important step to express the equilibrium described by the equations (A4-5) and (A6), especially (A4-5) with the Landau approximation.

A.2 *Approximations in the Numerical treatment*

The differential equations (A4) and (A5) were solved after application of the Hankel transform to r, Mellin transform to E and Laplace transform to t (Nishimura 1967, Kamata & Nishimura 1958). Retransformations from the solutions expressed in terms of complex functions required further approximated steps, the most important being the saddle point method. The final result expressed

in numerical densities was again fitted with a tolerable agreement with the so called NKG formula following an earliest Nishimura formula.

Another approach to solve the system of equations (A4-5) was performed by the method of adjoint equations (Lagutin et al. 1979 & Uchaikin et al. 1979) and the resulting structure functions were found steeper. Here also several numerical approximations had to make to get the solution.

Surprisingly, $\rho_{el}(r)$ which has not been checked above 10^{17} eV was used *in extensor* to calculate the radio synchrotron emission in giant extensive air showers (Suprun et al. 2003): recalculating those densities with *CORSIKA-EGS4*, we observed that the discrepancies remains small for axis distances lower than $3r_m$ containting fortunately the largest part of the source of radio emission or fluorescence in EAS.

A.3 *Analytic and Monte Carlo solutions*

The calculation of the electrons and photons spectra in shower of the same age obtained by Rossi and Greisen has the limitations that are intrinsic to the realistic but simplified theoretical framework (*Approximation B*) that has been used. This framework introduces several simplifications: the cross-sections for bremsstrahlung and pair-production have always the asymptotic form that is strictly speaking only valid at very high energy, the electron collision losses are treated as a simple energy independent constant, and Compton scattering is entirely neglected. Also in *Approximation B* the electron mass is neglected and the electron spectrum extends down to zero energy. A MC calculation of the spectral shapes can of course avoid all these limitations and is in principle more accurate, even if it has its own limitations and difficulties.

A comparison of the Rossi-Greisen shapes with the numerical results, show remarkable agreement but also some small differences, which could be interesting to explore in more detail. As an illustration, normalizing the high energy spectra to $\pi(E,s)) \rightarrow E^{-(s+1)}$, the quantity

$$s\int_0^\infty dE\pi_e(E,s) \qquad (A7)$$

is given by the function $K_1(s,-s)$ for the Rossi-Greisen calculation. The numerical integration of the Nerling *et al* parameterization (Giller et al. 2005 & Nerling et al.

2006) gives results that differ by 5 - 10 %. The parameterization for the electron spectrum has the form:

$$\pi_e(E,s) = \frac{1}{[E + a_1(s)][E + a_2(s)]^s} \qquad (A8)$$

that has manifestly the same asymptotic behaviour as the Rossi-Greisen shape at both low and high energy: $\pi_e(E) \rightarrow$ constant for $E \rightarrow 0$, and $\pi_e(E) \propto E^{-(s+1)}$ for $E \gg \varepsilon$ (ε being the critical energy).

For the Nerling parameterization the first coefficient is $c_1(s) = -[a_1(s) + sa_2(s)]$, which differs slightly from the coefficient as predicted from Rossi-Greisen solution beyond $s > 1$. The origin of the (small) difference between the analytic and MC solutions (i.e. numerical one) merits further studies. A possible explanation is a more precise description of the physics of the electromagnetic interactions in the MC calculation.

A.4 *Age parameter in longitudinal and lateral developments*

The shower age parameter (s) was first derived from the solution of equations (A1-2) using Mellin transformation, s being the variable in the complex plane. The total number of electrons (obtained by the inverse Mellin transformation) is obtained for $s = \bar{s}$ following the relation,

$$\lambda_1'(\bar{s})t + log\frac{E_0}{E} - \frac{1}{\bar{s}} = 0 \qquad (A9)$$

Taking into account the elementary solutions (where $\lambda_1'(\bar{s})$ is a function varying slowly), the relation between s and t was derived from the approximation at cascade maximum

$$\frac{\delta\bar{s}}{\delta t}\left(\lambda_1'(\bar{s})t + log\frac{E_0}{E} - \frac{1}{s}\right) + \lambda_1(\bar{s}) = 0 \qquad (A10)$$

and the general properties of s were established by the fact that the maximum of the cascade is at $s = 1$, the cascade is developing (growth) when $s \leq 1$, whereas it is decaying (absorption) if $s \geq 1$.

Those considerations in *Approximation B* are brought through the relation (**3.2**) for $s_{||}$, the so called Greisen formula for longitudinal development, along with

the relations (**3.1**) and (**3.4**). One of the clearest presentations of the qualitative relation between longitudinal shower age parameter and the lateral profile of the cascade under *Approximation B* was demonstrated by Cocconi (Cocconi 1961) showing that a lateral distribution is becoming flatter when $s \geq 1$ of course for $s_{||} = s_{\perp}$. The case of relation (**3.3**) for $s_{||}$ was also considered by Cocconi and Nishimura to take into account some effects of density resulting of the atmospheric inhomogeneity. Relation (**3.4**) has several advantages passing from an asymptotic tendency near axis when $r \to 0$ following r^{s-2} to a steeper power law when $r \to \infty$.

The problem of calculating the electron lateral distribution has attracted considerable in the past. Nishimura and Kamata solved numerically the 3-dimensional equations in *Approximation B* to obtain the (energy integrated) lateral distribution of electrons propagating in medium of constant density. Their results were fitted by Greisen (Greisen 1956 & 1960) with the approximate form:

$$\rho_{NKG}(r, s_{\perp}) = N_e f(r)_{NKG} = N_e C(s_{\perp})(\frac{r}{r_m})^{s_{\perp}-2}(1+\frac{r}{r_m})^{s_{\perp}-4.5} \quad (A11)$$

After these works several other authors have given different parameterization of the lateral distribution as a function of an age parameter.

The NKG function is based on the Eulerian Beta function, $B(u,v)$, taken here in the case of cylindrical symmetry, from:

$$N_e = \int_0^{\infty} 2\pi r \rho_{NKG}(r) dr \quad (A12)$$

$$= 2\pi C(s_{\perp}) \int_0^{\infty} (\frac{r}{r_m})^{s_{\perp}-1}(\frac{r}{r_m}+1)^{s_{\perp}-4.5} d\left(\frac{r}{r_m}\right) \quad (A13)$$

where appears the classical form:

$$B(u,v) = \int_0^{\infty} \frac{x^{u+1}}{(1+x)^{u+v}} dx \quad (A14)$$

for $x = \frac{r}{r_0}, u = s - 2 \; and \; v = 6.5 - 2s.$

This normalization via (A12) gives the opportunity to link one single density of electrons to $N_e$as

$$\rho_{NKG} = \frac{N_e}{r_m^2} f_{NKG}(r) \qquad (A15)$$

where $s_\perp$ must be a constant with respect to r corresponding to a fixed value of t in relation (**3.4**), otherwise expressing the integration in terms of Euler Beta function is not valid in general.

In reason of the difficulties observed with the experimental profile, the topological test of the local age parameter (equation **3.7**) was proposed to get an experimental hint of the validity of the lateral structure function. $s_\perp(r)$ is given automatically in the written output of ***CORSIKA*** option *NKG* for several axis distance (**User's Guide of *CORSIKA-6600/6970)***.

When the calculation of the electron component is carried out with relation (**3.6**), the situation with the *NKG* inspired procedure implemented in *CORSIKA* is more close to the experimental data and also of the calculation with *EGS4*.